

Scaling regimes and linear / nonlinear responses of last millennium climate to volcanic and solar forcings

S. Lovejoy¹, and C. Varotsos²

¹Physics, McGill University, 3600 University St., Montreal, Que., Canada

²Climate Research Group, Division of Environmental Physics and Meteorology, Faculty of Physics, University of Athens, University Campus Bldg. Phys. V, Athens 15784, Greece

Correspondence to: S. Lovejoy (lovejoy@physics.mcgill.ca) and C. Varotsos (covar@phys.uoa.gr)

Abstract. At scales much longer than the deterministic predictability limits (about 10 days), the statistics of the atmosphere undergoes a drastic transition, the high frequency weather acts as a random forcing on the lower frequency macroweather. In addition, up to decadal and centennial scales the equivalent radiative forcings of solar, volcanic and anthropogenic perturbations are small compared to the mean incoming solar flux. This justifies the common practice of reducing forcings to radiative equivalents (which are assumed to combine linearly), as well as the development of linear stochastic models, including for forecasting at monthly to decadal scales.

In order to clarify the validity of the linearity assumption and determine its scale range, we use last Millennium simulations, both with the simplified Zebiac- Cane (ZC) model and the NASA GISS E2-R fully coupled GCM. We systematically compare the statistical properties of solar only, volcanic only and combined solar and volcanic forcings over the range of time scales from one to 1000 years. We also compare the statistics to multiproxy temperature reconstructions. The main findings are: a) that the variability of the ZC and GCM models are too weak at centennial and longer scales, b) for longer than ≈ 50 years, the solar and volcanic forcings combine subadditively (nonlinearly) compounding the weakness of the response, c) the models display another nonlinear effect at shorter time scales: their sensitivities are much higher for weak forcing than for strong forcing (their intermittencies are different) and we quantify this with statistical scaling exponents.

26 **1. Introduction**

27 **1.1 Linearity versus nonlinearity**

28 The GCM approach to climate modeling is based on the idea that whereas weather is an initial value
29 problem, the climate is a boundary value problem (Bryson, 1997; Pielke, 1998). This means that although
30 the weather's sensitive dependence on initial conditions (chaos, the "butterfly effect") leads to a loss of
31 predictability at time scales of about 10 days, nevertheless averaging over enough "weather" leads to a
32 convergence to the model's "climate". This climate is thus the state to which averages of model outputs
33 converge for fixed atmospheric compositions and boundary conditions (i.e. control runs).

34 The question then arises as to the response of the system to small changes in the boundary conditions:
35 for example anthropogenic forcings are less than 2 W/m^2 , and at least over scales of several years, solar and
36 volcanic forcings are of similar magnitude or smaller (see e.g. Fig. 1a and the quantification in Fig. 2).
37 These numbers are of the order of 1% of the mean solar radiative flux so that we may anticipate that the
38 atmosphere responds fairly linearly. This is indeed that usual assumption and it justifies the reduction of
39 potentially complex forcings to overall radiative forcings (see Meehl et al., 2004 for GCM investigations at
40 annual scales and Hansen et al., 2005 for greenhouse gases). However, at long enough scales, linearity
41 clearly breaks down, indeed starting with the celebrated "Daisy world" model (Watson and Lovelock,
42 1983), there is a whole literature that uses energy balance models to study the strongly nonlinear
43 interactions/feedbacks between global temperatures and albedoes. There is no debate that temperature-
44 albedo feedbacks are important at the multimillennial scales of the glacial- interglacial transitions. While
45 some authors (e.g. Roques et al., 2014) use time scales as short as 200 years for the critical ice-albedo
46 feedbacks, others have assumed that the temperature response to solar and volcanic forcings over the last
47 millennium are reasonably linear (e.g. Østvand et al., 2014; Rypdal and Rypdal, 2014), while Pelletier
48 (1998) and Fraedrich et al., (2009) assume linearity to even longer scales.

49 It is therefore important to establish the times scales over which linear responses are a reasonable
50 assumption. However, clearly even over scales where typical responses to small forcings are relatively
51 linear, the response may be nonlinear if the forcing is – volcanic or volcanic- like, i.e. if it is sufficiently
52 "spikey" or intermittent.

53 **1.2 Atmospheric variability: scaling regimes**

54 Before turning our attention to models, what can we learn empirically? Certainly, at high enough
55 frequencies (the weather regime), the atmosphere is highly nonlinear. However, at about ten days, the

56 atmosphere undergoes a drastic transition to a lower frequency regime, and this “macroweather”
 57 regime is potentially quasi- linear in its responses. Indeed, the basic atmospheric scaling regimes were
 58 identified some time ago - primarily using spectral analysis (Lovejoy and Schertzer, 1986; Pelletier, 1998;
 59 Shackleton and Imbrie, 1990; Huybers and Curry, 2006). However, the use of real space fluctuations
 60 provided a clearer picture and a simpler interpretation. It also showed that the usual view of atmospheric
 61 variability, as a sequence of narrow scale range processes (e.g. nonlinear oscillators), has seriously
 62 neglected the main source of variability, namely the scaling “background spectrum” (Lovejoy, 2014). What
 63 was found is that for virtually all atmospheric fields, there was a transition from the behavior of the mean
 64 temperature fluctuations scaling $\langle \Delta T(\Delta t) \rangle \approx \Delta t^H$ with $H > 0$ to a lower frequency scaling regime with $H < 0$ at
 65 scales $\Delta t \gtrsim 10$ days; the macroweather regime. The transition scale of around 10 days, can be theoretically
 66 predicted on the basis of the scaling of the turbulent wind due to solar forcing (via the imposed energy rate
 67 density; see (Lovejoy and Schertzer, 2010; Lovejoy and Schertzer, 2013; Lovejoy et al., 2014). Whereas
 68 the weather is naturally identified with the high frequency $H > 0$ regime and with temperature values
 69 “wandering” up and down like a drunkard’s walk, the lower frequency $H < 0$ regime is characterized by
 70 fluctuations tending to cancel out – effectively starting to converge. This converging regime is a low
 71 frequency type of weather, described as “macroweather” (Lovejoy, 2013; Lovejoy et al., 2014). For the
 72 GCM control runs, macroweather effectively continues to asymptotically long times; in the real world, it
 73 continues to time scales of 10-30 years (industrial) and 50-100 years (pre-industrial) after which a new $H > 0$
 74 regime is observed; it is natural to associate this new regime with the climate (see Fig. 5 of Lovejoy et al.,
 75 2013; see also Franzke et al., 2013). Other papers analyzing macroweather scaling include Koscielny-
 76 Bunde et al., (1998); Eichner et al., (2003); Kantelhardt et al., (2006); Rybski et al., (2006); Bunde et al.,
 77 (2005); Østvand et al., (2014); Rypdal and Rypdal, (2014); Fredriksen and Rypdal, (2015).

78 The explanation for the “macroweather” to climate transition (at scale τ_c) appears to be that over the
 79 “macroweather” time scales - where the fluctuations are “cancelling” - other, slow processes which
 80 presumably include both external climate forcings and other slow (internal) land-ice or biogeochemical
 81 processes – become stronger and stronger. At some point (τ_c) their variability dominates. A significant
 82 point where opinions diverge is the value of the global transition scale τ_c during the preindustrial Holocene;
 83 and the possibility that there are large regional variations in τ_c during the Holocene so that Greenland ice
 84 core data may not be globally representative, see Lovejoy (2015a) for a discussion.

85 **1.3 Scaling in the numerical models**

86 There have been several studies of the low frequency control run responses of GCMs (Vyushin et
87 al., 2004; Zhu et al., 2006; Fraedrich et al., 2009; Lovejoy et al., 2013; Fredriksen and Rypdal, 2015)
88 finding that they are scaling down to their lowest frequencies. This scaling is a consequence of the absence
89 of a characteristic time scale for the long-time model convergence; it turns out that the relevant scaling
90 exponents are very small: empirically the GCM convergence is “ultra slow” (Lovejoy et al., 2013) (section
91 3.4). Most earlier studies focused on the implications of the long – range statistical dependencies implicit in
92 the scaling statistics. Unfortunately, due to this rather technical focus, the broader implications of the
93 scaling have not been widely appreciated.

94 More recently, using scaling fluctuation analysis, behavior has been put into the general theoretical
95 framework of GCM climate modeling (Lovejoy et al., 2013). From the scaling point of view, it appears that
96 the climate arises as a consequence of slow internal climate processes combined with external forcings
97 (especially volcanic and solar - and in the recent period - anthropogenic forcings). From the point of view
98 of the GCMs, the low frequency (multicentennial) variability arises exclusively as a response to external
99 forcings, although potentially - with the addition of (known or currently unknown) slow processes such as
l00 land-ice or biogeochemical processes - new internal sources of low frequency variability could be included.
l01 Ignoring the recent (industrial) period, and confining ourselves to the last millennium, the key question for
l02 GCM models is whether or not they can reproduce the climate regime where the decline of the
l03 “macroweather” fluctuations ($H < 0$) is arrested and the increasing $H > 0$ climate regime fluctuations begin. In
l04 a recent publication (Lovejoy et al., 2013), four GCMs simulating the last millennium were statistically
l05 analyzed and it was found that their low frequency variability (especially below $(100 \text{ yrs})^{-1}$) was somewhat
l06 weak, and this was linked to both the weakness of the solar forcings (when using sunspot-based solar
l07 reconstructions with $H > 0$), and – for strong volcanic forcings - with the statistical type of the forcing ($H < 0$,
l08 Lovejoy and Schertzer, 2012a; Bothe et al., 2013a,b; Zanchettin et al., 2013; see also Zanchettin et al., 2010
l09 for the dynamics on centennial time scales).

l10 **1.4 This paper**

l11 The weakness of the responses to solar and volcanic forcings at multicentennial scales raises question a
l12 linearity question: is the response of the combined (solar plus volcanic) forcing roughly the sum of the
l13 individual responses? Additivity is often implicitly assumed when climate forcings are reduced to their
l14 equivalent radiative forcings and Mann et al., (2005) already pointed out that – at least - in the Zebiac-Cane
l15 (ZC) model discussed below that they are not additive. Here we more precisely analyze this question and
l16 quantify the degree of sub-additivity as a function of temporal scale (section 3.4). A related linear/nonlinear

l17 issue pointed out by Clement et al., (1996), is that due to the nonlinear model response, there is a
l18 high sensitivity to a small forcing and a low sensitivity to a large forcing. Systems in which strong and
l19 weak events have different statistical behaviors display stronger or weaker “clustering” and are often
l20 termed “intermittent” (from turbulence). When they are also scaling, the weak and strong events are
l21 characterized by different scaling exponents that quantify how the respective clustering changes with scale.
l22 In section 4, we investigate this quantitatively and confirm that it is particularly strong for volcanic forcing,
l23 and that for the ZC model the response (including that of a GCM), is much less intermittent, implying that
l24 the model strongly (and nonlinearly) smooths the forcing.

l25 In this paper, we establish analysis methodologies that can address these issues and apply them to
l26 model outputs that cover the the required range of time scales: Last Millenium model outputs.
l27 Unfortunately - although we consider the NASA GISS E2-R Last Millenium simulations, there seem to be
l28 no full Last Millenium GCM simulations that have the entire suite of volcanic only, solar only and solar
l29 plus volcanic forcings and responses, therefore we have use the simplified Zebiak-Cane model outputs
l30 published by Mann et al., (2005) (and even this lacked control runs to directly quantify the internal
l31 variability).

l32 Although the Zebiak –Cane model lacks several important mechanisms- notably for our purposes
l33 deep ocean dynamics - there are clearly sources of low frequency variability present in the model. For
l34 example, Goswami and Shukla, (1991) using 360 year control runs found multidecadal and multicentennial
l35 nonlinear variability due to the feedbacks between SST anomalies, low level convergence and atmospheric
l36 heating. In addition, in justifying his Millenium ZC simulations, (Mann et al., 2005) specifically cited
l37 model centennial scale variability as a factor motivating their study.

l38 **2. Data and analysis**

l39 **2.1 Discussion**

l40 During the pre-industrial part of the last millennium, the atmospheric composition was roughly constant,
l41 and the earth’s orbital parameters varied by only a small amount. The main forcings used in GCM climate
l42 models over this period are thus solar and volcanic (in the GISS-E2-R simulations discussed below,
l43 reconstructed land use changes are also simulated but the corresponding forcings are comparatively weak
l44 and will not be discussed further). In particular, the importance of volcanic forcings was demonstrated by
l45 Minnis et al., (1993) who investigated the volcanic radiative forcing caused by the 1991 eruption of Mount
l46 Pinatubo, and found that volcanic aerosols produced a strong cooling effect. Later, Shindell et al., (2003)

l47 used a stratosphere-resolving general circulation model to examine the effect of the volcanic
l48 aerosols and solar irradiance variability on pre-industrial climate change. They found that the best
l49 agreement with historical and proxy data was obtained using both forcings. However, solar and volcanic
l50 forcings induce different responses because the stratospheric and surface influences in the solar case
l51 reinforce one another but in the volcanic case they are opposed. In addition, there are important differences
l52 in solar and volcanic temporal variabilities (including seasonality) that statistically link volcanic eruptions
l53 with the onset of ENSO events (Mann et al., 2005). Decreased solar irradiance cools the surface and
l54 stratosphere (Cracknell and Varotsos 2007, 2011; Kondratyev and Varotsos, 1995a,b). In contrast, volcanic
l55 eruptions cool the surface, but aerosol heating warms the sunlit lower stratosphere (Shindell et al., 2003;
l56 Miller et al., 2012). This leads to an increased meridional gradient in the lower stratosphere, but a reduced
l57 gradient in the tropopause region (Chandra et al., 1996; Varotsos et al., 1994, 2009).

l58 Vyushin et al., (2004) suggested that volcanic forcings improve the low frequency variability scaling
l59 performance of atmosphere-ocean models compared to all other forcings (see however the comment by
l60 Blender and Fraedrich, (2004), which also discusses earlier papers on the field e.g. Fraedrich and Blender,
l61 (2003); Blender and Fraedrich, (2004). Weber, (2005) used a set of simulations with a climate model,
l62 driven by reconstructed forcings in order to study the Northern Hemisphere temperature response to
l63 volcanic and solar forcing, during 1000-1850. It was concluded that the response to solar forcing
l64 equilibrates at interdecadal timescales, while the response to volcanic forcing never equilibrates due to the
l65 fact that the time interval between volcanic eruptions is typically shorter than the dissipation time scale of
l66 the climate system (in fact they are scaling so that eruptions occur over all observed time scales, see
l67 below).

l68 At the same time, Mann et al. (2005) investigated the response of El Niño to natural radiative forcing
l69 changes during 1000-1999, by employing the Zebiak–Cane model for the coupled ocean–atmosphere
l70 system in the tropical Pacific. They found that the composite feedback of the volcanic and solar radiative
l71 forcing to past changes, reproduces the fluctuations in the variability of the historic El Niño records (e.g.,
l72 Efstathiou et al., 2011; Varotsos 2013).

l73 Finally, as discussed below Lovejoy and Schertzer, (2012a) analysed the time scale dependence of
l74 several solar reconstructions Lean, (2000); Wang et al., (2005); Krivova et al., (2007); Steinhilber et al.,
l75 (2009); Shapiro et al., (2011) and the two main volcanic reconstructions Crowley, (2000) and Gao et al.,
l76 (2008), (referred to as “Crowley” and “Gao” in the following). The solar forcings were found to be
l77 qualitatively quite different depending on whether the reconstructions were based on sunspots or ¹⁰Be
l78 isotopes from ice cores with the former increasing with time scale and the latter decreasing with time scale.

179 This quantitative and qualitative difference brings into question the reliability of the solar
 180 reconstructions. By comparison, the two volcanic reconstructions were both statistically similar in type;
 181 they were very strong at annual and sometimes multiannual scales but they quickly decrease with time
 182 scale ($H < 0$) explaining why they are weak at centennial and millennial scales. We re-examine these
 183 findings below.

184 2.2 The climate simulation of Mann et al. (2005) using the Zebiak-Cane model

185 Mann et al., (2005) used the Zebiak–Cane model of the tropical Pacific coupled ocean – atmosphere system
 186 (Zebiak and Cane, 1987) to produce a 100-realization ensemble for solar forcing only, volcanic forcing
 187 only and combined forcings over the last millennium. Figure 1a shows the forcings and mean responses of
 188 the model which were obtained from:
 189 ftp://ftp.ncdc.noaa.gov/pub/data/paleo/climate_forcing/mann2005/mann2005.txt. No anthropogenic effects
 190 were included. Mann et al., (2005) modeled the region between $\pm 30^\circ$ of latitude - by scaling the Crowley
 191 volcanic forcing reconstruction with a geometric factor 1.57 to take the limited range of latitudes into
 192 account. Figure 1b shows the corresponding GISS-E2-R simulation responses for three different forcings as
 193 discussed in Schmidt et al., (2013) and Lovejoy et al., (2013). Although these were averaged over the
 194 northern hemisphere land only (a somewhat different geography than the ZC simulations), one can see that
 195 the low frequencies seem similar even if the high frequencies are somewhat different. We quantify this
 196 below.

197 3. Methods

198 3.1 Comparing simulations with observations as functions of scale

199 The ultimate goal of weather and climate modelling (including forecasting) is to make simulations $T_{sim}(t)$
 200 as close as possible to observations $T_{obs}(t)$. Ignoring measurement errors and simplifying the discussion by
 201 only considering a single spatial location (i.e. a single time series), the goal is to achieve simulations with
 202 $T_{sim}(t) = T_{obs}(t)$. However, this is not only very ambitious for the simulations, even when considering the
 203 observations, $T_{obs}(t)$ is often difficult to evaluate if only because data are often sparse or inadequate in
 204 various ways. However, a necessary condition for $T_{sim}(t) = T_{obs}(t)$ is the weaker statistical equality: $T_{sim}(t) \stackrel{d}{=} T_{obs}(t)$
 205 where “ $\stackrel{d}{=}$ ” means equal in probability distributions (we can say that $a \stackrel{d}{=} b$ if $\Pr(a > s) = \Pr(b > s)$ where “Pr”

206 indicates “probability”). Although $T_{sim}(t) \stackrel{d}{=} T_{obs}(t)$ is only a necessary (but not sufficient) condition
 207 for $T_{sim}(t) = T_{obs}(t)$, it is much easier to empirically verify.

208 Starting in the 1990s, with the advent of ensemble forecasting systems, the Rank Histogram (RH)
 209 method was proposed (Anderson, 1996) as a simple nonparametric test of $T_{sim}(t) \stackrel{d}{=} T_{obs}(t)$, and this has led
 210 to a large literature, including recently Bothe et al., (2013a, b). From our perspective there are two
 211 limitations of the RH method. First, it is non-parametric so that its statistical power is low. More
 212 importantly, it essentially tests the equation $T_{sim}(t) \stackrel{d}{=} T_{obs}(t)$ at a single unique time scale/resolution. This is
 213 troublesome since the statistics of both $T_{sim}(t)$ and $T_{obs}(t)$ series will depend on their space-time
 214 resolutions; recall that averaging in space alters the temporal statistics, e.g. $5^0 \times 5^0$ data are not only spatially,
 215 but also are effectively temporally smoothed with respect to $1^0 \times 1^0$ data. This means that even if $T_{sim}(t)$ and
 216 $T_{obs}(t)$ have nominally the same temporal resolutions they may easily have different high frequency
 217 variability. Possibly more importantly - as claimed in Lovejoy et al., (2013) and below - the main
 218 difference between $T_{sim}(t)$ and $T_{obs}(t)$ may be that the latter has more low frequency variability than the
 219 former, and this will not be captured by the RH technique which operates only at the highest frequency
 220 available. This problem is indirectly acknowledged, see for example the discussion of correlations in
 221 Marzban et al., (2011). The potential significance of the low frequencies becomes obvious when $H > 0$ for
 222 the low frequency range. In this case – since the series tends to “wander”, small differences in the low
 223 frequencies may translate into very large differences in RH, and this even if the high frequencies are
 224 relatively accurate.

225 A straightforward solution is to use the same basic idea – i.e. to change the sense of equality from
 226 deterministic to probabilistic (“=” to “ $\stackrel{d}{=}$ ”) – but to compare the statistics systematically over a range of
 227 time scales. The simplest way is to check the equality $\Delta T_{sim}(\Delta t) \stackrel{d}{=} \Delta T_{obs}(\Delta t)$ where ΔT is the fluctuation of the
 228 temperature over a time period Δt (see the discussion in Lovejoy and Schertzer, (2013) box 11.1). In
 229 general, knowledge of the probabilities is equivalent to knowledge of (all) the statistical moments
 230 (including the non-integer ones), and for technical reasons it turns out to be easier to check
 231 $\Delta T_{sim}(\Delta t) \stackrel{d}{=} \Delta T_{obs}(\Delta t)$ by considering the statistical moments.

232 3.2 Scaling Fluctuation Analysis

233 In order to isolate the variability as a function of time scale Δt , we estimated the fluctuations $\Delta F(\Delta t)$
 234 (forcings, W/m^2), $\Delta T(\Delta t)$ (responses, K). Although it is traditional (and often adequate) to define
 235 fluctuations by absolute differences $\Delta T(\Delta t) = |T(t+\Delta t) - T(t)|$, for our purposes this is not sufficient. Instead we
 236 should use the absolute difference of the means from t to $t+\Delta t/2$ and from $t+\Delta t/2$ to $t+\Delta t$. Technically, the
 237 latter corresponds to defining fluctuations using Haar wavelets rather than “poor man’s” wavelets
 238 (differences). In a scaling regime, the fluctuations vary with the time lag in a power law manner:

$$239 \quad \Delta T = \varphi \Delta t^H \quad (1)$$

240
 241 where φ is a controlling dynamical variable (e.g. a dynamical flux) whose mean $\langle \varphi \rangle$ is independent of the
 242 lag Δt (i.e. independent of the time scale). This means that the behaviour of the mean fluctuation is
 243 $\langle \Delta T \rangle \approx \Delta t^H$ so that when $H > 0$, on average fluctuations tend to grow with scale whereas when $H < 0$, they tend
 244 to decrease. Note that the symbol “ H ” is in honour of Harold Edwin Hurst (Hurst, 1951). Although in the
 245 case of quasi-Gaussian statistics, it is equal to his eponymous exponent, the H used here is valid in the more
 246 general multifractal case and is generally different.

247 Fluctuations defined as differences are adequate for fluctuations increasing with scale ($H > 0$).
 248 When $H > 0$, the rate at which average differences increase with time lag Δt directly reflects the increasing
 249 importance of low frequencies with respect to high frequencies. However, in physical systems the
 250 differences tend to increase even when $H < 0$. This is because correlations $\langle T(t+\Delta t)T(t) \rangle$ tend to decrease
 251 with the time lag Δt and this directly implies that the mean square differences $\langle (\Delta T(\Delta t))^2 \rangle$ increase
 252 (mathematically, for a stationary process: $\langle \Delta T(\Delta t)^2 \rangle = \langle (T(t+\Delta t) - T(t))^2 \rangle = 2(\langle T^2 \rangle - \langle T(t+\Delta t)T(t) \rangle)$). This means that
 253 when $H < 0$, differences cannot correctly characterize the fluctuations. For $H < 0$ the high-frequency details
 254 dominate the differences and prevent these differences to decrease with increasing scale Δt .

255 The Haar fluctuation which is useful for $-1 < H < 1$ is particularly easy to understand since with proper
 256 “calibration” in regions where $H > 0$, its value can be made to be very close to the difference fluctuation,
 257 while in regions where $H < 0$, it can be made close to another simple to interpret “anomaly fluctuation”. The
 258 latter is simply the temporal average of the series over a duration Δt of the series with its overall mean
 259 removed (in Lovejoy and Schertzer, 2012b this was termed a “tendency” fluctuation which is a less
 260 intuitive term). In this case, the decrease of the Haar fluctuations for increasing lag Δt characterizes how
 261 effectively averaging a (mean zero) process (the anomaly) over longer time scales reduces its variability.

262 Here, the calibration is affected by multiplying the raw Haar fluctuation by a factor of 2 which
 263 brings the values of the Haar fluctuations very close to both the corresponding difference and anomaly
 264 fluctuations (over time scales with $H > 0$, $H < 0$ respectively). This means that in regions where $H > 0$, to good
 265 accuracy, the Haar fluctuations can be treated as differences whereas in regions where $H < 0$ they can be
 266 treated as anomalies. While other techniques such as Detrended Fluctuation Analysis (Peng et al., 1994)
 267 perform just as well for determining exponents, they have the disadvantage that their fluctuations are not at
 268 all easy to interpret (they are the standard deviations of the residues of polynomial regressions on the
 269 running sum of the original series). Indeed, the DFA fluctuation function is typically presented without any
 270 units.

271 Once estimated, the variation of the fluctuations with time scale can be quantified by using their
 272 statistics; the q^{th} order structure function $S_q(\Delta t)$ is particularly convenient:

$$273 \quad S_q(\Delta t) = \left\langle \Delta T(\Delta t)^q \right\rangle \quad (2)$$

274 where “ $\langle \rangle$ ” indicates ensemble averaging (here, we average over all disjoint intervals of length Δt). Note
 275 that although q can in principle be any value, here we restrict to $q > 0$ since divergences may occur – indeed
 276 for multifractals, are expected - for $q < 0$). In a scaling regime, $S_q(\Delta t)$ is a power law:

$$278 \quad S_q(\Delta t) = \left\langle \Delta T(\Delta t)^q \right\rangle \propto \Delta t^{\xi(q)}; \quad \xi(q) = qH - K(q) \quad (3)$$

279 where the exponent $\xi(q)$ has a linear part qH and a generally nonlinear and convex part $K(q)$ with $K(1)=0$.
 280 $K(q)$ characterizes the strong non Gaussian, multifractal variability; the “intermittency”. Gaussian processes
 281 have $K(q)=0$. The root-mean-square (RMS) variation $S_2(\Delta t)^{1/2}$ (denoted simply $S(\Delta t)$ below) has the
 282 exponent $\xi(2)/2 = H - K(2)/2$. It is only when the intermittency is small ($K(q) \approx 0$) that we have
 283 $\xi(2)/2 \approx H = \xi(1)$. Note that since the spectrum is a second order statistic, we have the useful relationship for
 284 the exponent β of the power law spectra: $\beta = 1 + \xi(2) = 1 + 2H - K(2)$ (this is a corollary of the Wiener-Khintchin
 285 theorem). Again, only when $K(2)$ is small do we have the commonly used relation $\beta \approx 1 + 2H$; in this case, $H > 0$,
 286 $H < 0$ corresponds to $\beta > 1$, $\beta < 1$, respectively. To get an idea of the implications of the nonlinear $K(q)$, note
 287 that a high q value characterizes the scaling of the strong events whereas a low q characterizes the scaling
 288 of the weak events (q is not restricted to integer. The scalings are different whenever the strong and weak
 289 events cluster to different degrees, the clustering in turn is precisely determined by another exponent - the

290 codimension - which is itself is uniquely determined by $K(q)$. We return to the phenomenon of
 291 “intermittency”, in section 4, it is particularly pronounced in the case of volcanic forcings.

292 Figure 2a shows the result of estimating the Haar fluctuations for the solar and volcanic forcings. The
 293 solar reconstruction that was used is a hybrid obtained by “splicing” the annual resolution sunspot based
 294 reconstruction (Fig. 2b, top; back to 1610, although only the more recent part was used by Mann et al.
 295 (2005) with a ^{10}Be based reconstruction (Fig. 2b, bottom) at much lower resolution ($\approx 40\text{-}50$ yrs). In Fig. 2a,
 296 the two rightmost curves are for two different ^{10}Be reconstructions; at any given time scale, their
 297 amplitudes differ by nearly a factor of 10 yet they both have Haar fluctuations that diminish with scale
 298 ($H \approx -0.3$). Figure 2b (top) clearly shows the qualitative difference with “wandering” ($H > 0$, sunspot based)
 299 and Fig. 2b (bottom), the cancelling ($H < 0$, ^{10}Be based) solar reconstructions (Lovejoy and Schertzer,
 300 2012a). In the “spliced” reconstruction used here, the early ^{10}Be part (1000-1610) at low resolution was
 301 interpolated to annual resolution; the interpolation was close to linear so that we find $H \approx 1$ over the scale
 302 range 1-50 yrs, with the $H < 0$ part barely visible over the range 100-600 years (roughly the length of the
 303 ^{10}Be part of the reconstruction).

304 The reference lines in Fig. 2a have slopes -0.4, -0.3, 0.4 showing that both solar and volcanic forcings
 305 are fairly accurately scaling (although because of the “splicing” for the solar, only up until $\approx 200\text{-}300$ yrs)
 306 but with exactly opposite behaviours: whereas the solar fluctuations increase with time scale, the volcanic
 307 fluctuations decrease with scale. For time scales beyond 200-300 yrs, the solar forcing is stronger than the
 308 volcanic forcing (they “cross” at roughly 0.3 W/m^2).

309 3.3 Linearity and nonlinearity

310 There is no question that - at least in the usual deterministic sense - the atmosphere is turbulent and
 311 nonlinear. Indeed, the ratio of the nonlinear to the linear terms in the dynamical equations – the Reynolds
 312 number - is typically about 10^{12} . Due to the smaller range of scales, in the numerical models it is much
 313 lower, but it is still $\approx 10^3$ to 10^4 . Indeed it turns out that the variability builds up scale by scale from large to
 314 small scales so that - since the dissipation scale is about 10^{-3} m - the resulting (millimetre scale) variability
 315 can be enormous; the statistics of this buildup are quite accurately modelled by multifractal cascades (see
 316 the review Lovejoy and Schertzer, 2013, especially ch. 4 for cascade analyses of data and model outputs).
 317 The cascade based Fractionally Integrated Flux model (FIF, Schertzer and Lovejoy, 1987) is a nonlinear
 318 stochastic model of the weather scale dynamics, and can be extended to provide nonlinear stochastic
 319 models of the macroweather and climate regimes (Lovejoy and Schertzer, 2013, ch. 10).

320 However, ever since Hasselmann, (1976), it has been proposed that sufficiently space-time
 321 averaged variables may respond linearly to sufficiently space-time averaged forcings. In the resulting (low
 322 frequency) phenomenological models, the nonlinear deterministic (high frequency) dynamics act as a
 323 source of random perturbations; the resulting stochastic model is usually taken as being linear. Such models
 324 are only justified if there is a physical scale separation between the high frequency and low frequency
 325 processes. The existence of a relevant break (at 2- 10 day scales) has been known since Panofsky and Van
 326 der Hoven, (1955) and was variously theorized as the “scale of migratory pressure systems of synoptic
 327 weather map scale” (Van der Hoven, 1957) and later as the “synoptic maximum” (Kolesnikov and Monin,
 328 1965). From the point of view of Hasselman-type linear stochastic modelling (now often referred to as
 329 “Linear Inverse Modelling (LIM)”, e.g., Penland and Sardeshmukh, (1995); Newman et al., (2003);
 330 Sardeshmukh and Sura, (2009)), the system is regarded as a multivariate Ornstein-Uhlenbeck (OU) process.
 331 At high frequencies, an OU process is essentially the integral of a white noise (with spectrum $\omega^{-\beta_h}$ with
 332 $\beta_h = 2$), whereas at low frequencies it is a white noise, (i.e. $\omega^{-\beta_l}$ with $\beta_l = 0$). In the LIM models, these
 333 regimes correspond to the weather and macroweather, respectively. Recently Newman, (2013) has shown
 334 predictive skill for global temperature hindcasts is somewhat superior to GCM’s for 1-2 year horizons.

335 In the more general scaling picture going back to Lovejoy and Schertzer, (1986), the transition
 336 corresponds to the lifetime of planetary structures. This interpretation was quantitatively justified in
 337 (Lovejoy and Schertzer, 2010) by using the turbulent energy rate density. The low and high frequency
 338 regimes were scaling and had spectra significantly different than those of OU processes (notably with $0.2 <$
 339 $\beta_l < 0.8$) with the two regimes now being referred to as “weather” and “macroweather” (Lovejoy and
 340 Schertzer, 2013). Indeed, the main difference with respect to the classical LIM is at low frequencies.
 341 Although the difference in β_l may not seem so important, the LIM value $\beta_l = 0$, (white noise) has no low
 342 frequency predictability whereas the actual values $0.2 < \beta_l < 0.8$ (depending mostly on the land or ocean
 343 location) corresponds to potentially huge predictability (the latter can diverge as β_l approaches 1). A new
 344 “ScaLIing Macroweather Model” (SLIMM) has been proposed as a set of fractional order (but still linear)
 345 stochastic differential equations with predictive skill for global mean temperatures out to at least 10 years
 346 (Lovejoy et al., 2015; Lovejoy, 2015b). However, irrespective of the exact statistical nature of the weather
 347 and macroweather regimes, a linear stochastic model may still be a valid approximation over significant
 348 ranges.

349 These linear stochastic models (whether LIM or SLIMM) explicitly exploit the weather/macroweather
 350 transition and may have some skill up to macroweather scales perhaps as large as decades. However, at

351 long enough time scales, another class of phenomenological model is often used, wherein the
 352 dynamics are determined by radiative energy balances. Energy balance models focus on slower (true)
 353 climate scale processes such as sea ice – albedo feedbacks and are generally quite nonlinear, being
 354 associated with nonlinear features such as tipping points and bifurcations (Budyko, 1969). These models
 355 are typically zero or one dimensional in space (i.e. they are averaged over the whole earth or over latitude
 356 bands) and may be deterministic or stochastic (see Nicolis, 1988 for an early comparison of the two
 357 approaches). See Dijkstra, (2013) for a survey of the classical deterministic dynamical systems approach as
 358 well as the more recent stochastic “random dynamical systems” approach, (see also Ragone, et al., 2014).
 359 Although energy balance models are almost always nonlinear, there have been several suggestions that
 360 linear energy balance models are in fact valid up to millennial and even multimillennial scales.

361 Finally, we could mention the existence of empirical evidence of stochastic linearity between
 362 forcings and responses in the macroweather regime. Such evidence comes for example, from the apparent
 363 ability of linear regressions to “remove” the effects of volcanic, solar and anthropogenic forcings (Lean and
 364 Rind, 2008). This has perhaps been quantitatively demonstrated in the case of anthropogenic forcing where
 365 use is made of the globally, annually averaged CO₂ radiative forcings (as a linear surrogate for all
 366 anthropogenic forcings). When this radiative forcing was regressed against similarly averaged temperatures,
 367 it gave residues with amplitudes $\pm 0.109\text{K}$ (Lovejoy, 2014a) which is almost exactly the same as GCM
 368 estimates of the natural variability (e.g., Laepple et al., (2008)). Notice that in this case the identification of
 369 the global temperature T_{globe} as the sum of a regression determined anthropogenic component (T_{anth}) with
 370 residues as natural variability (T_{nat}) is in fact only a confirmation of *stochastic* linearity (i.e.
 371 $T_{globe} \stackrel{d}{=} T_{anth} + T_{nat}$). Since presumably the actual residues would have been different if there had been no
 372 anthropogenic forcing. Indeed, when the residues were analysed using fluctuation analysis, it was only their
 373 statistics that were close to the pre-industrial multiproxy statistics.

374 **3.4 Testing linearity: the additivity of the responses**

375 We can now test the linearity of the model responses to solar and volcanic forcings. First consider the
 376 model responses (Fig. 3a). Compare the response to the volcanic only forcing (green) curve; with the
 377 response from the solar only forcing (black). As expected from Fig. 2a, the former is stronger than the latter
 378 up (until centennial scales) reflecting the stronger volcanic forcing. At scales $\Delta t \approx 100$ yrs however, we
 379 see that the solar only has a stronger response, also as expected from Fig. 2a. Now consider the response to
 380 the combined volcanic and solar forcing (brown). Unsurprisingly, it is very close to the volcanic only until

381 $\Delta t \approx 100$ yrs; however at longer time scales, the combined response seems to decrease following
 382 the volcanic forcing curve; it seems that at these longer time scales the volcanic and solar forcings have
 383 negative feedbacks so that the combined response to solar plus volcanic forcing is actually less than for
 384 pure solar forcing, they are “subadditive”.

385 In order to quantify this we can easily determine the expected solar and volcanic response if the two
 386 were combined additively (linearly). In the latter case, the solar and volcanic fluctuations would not
 387 interfere with each other, and since these forcings are statistically independent, the responses would also be
 388 statistically independent, the response variances would add.

389 A linear response means that temperature fluctuations due to only solar forcing ($\Delta T_s(\Delta t)$) and only
 390 volcanic forcing ($\Delta T_v(\Delta t)$) would be related to the temperature fluctuations of the response to the
 391 combined solar plus volcanic forcings ($\Delta T_{s,v}(\Delta t)$) as:

$$392 \quad \Delta T_{s,v}(\Delta t) = \Delta T_s(\Delta t) + \Delta T_v(\Delta t) \quad (4)$$

393 This is true regardless of the exact definition of the fluctuation: as long as the fluctuation is defined by a
 394 linear operation on the temperature series any wavelet will do. Therefore, squaring both sides and
 395 averaging (“ $\langle \rangle$ ”) and assuming that the fluctuations in the solar and volcanic forcings are statistically
 396 independent of each other (i.e., $\langle \Delta T_s(\Delta t) \Delta T_v(\Delta t) \rangle = 0$), we obtain:

$$397 \quad \langle \Delta T_{s,v}(\Delta t)^2 \rangle = \langle \Delta T_s(\Delta t)^2 \rangle + \langle \Delta T_v(\Delta t)^2 \rangle \quad (5)$$

398 The implied additive response structure function $S(\Delta t) = \left(\langle \Delta T_s(\Delta t)^2 \rangle + \langle \Delta T_v(\Delta t)^2 \rangle \right)^{1/2}$ is shown in Fig. 3b along
 399 with the ratio of the latter to the actual (nonlinear) solar plus volcanic response (top:
 400 $\left(\langle \Delta T_s(\Delta t)^2 \rangle + \langle \Delta T_v(\Delta t)^2 \rangle \right)^{1/2} / \langle \Delta T_{s,v}(\Delta t)^2 \rangle^{1/2}$). It can be seen that the ratio is fairly close to unity for time scales below
 401 about 50 yrs. However beyond 50 yrs there is indeed a strong negative feedback between the solar and
 402 volcanic forcings. This is seen more clearly in Fig. 3c which shows that at $\Delta t \approx 400$ years, that the negative
 403 feedback is strong enough to reduce the theoretical additive fluctuation amplitudes by a factor of ≈ 2 (the
 404 fall-off at the largest Δt is probably an artefact of the poor statistics at these scales). It should be noted that
 405 in addition to linearity, the latter holds assuming statistical independence (top curve in Fig. 3c) of the solar
 406 and volcanic forcing. For comparison, the bottom curve in Fig. 3c illustrates the results obtained when
 407 analyzing the series constructed by directly summing the two response series (instead of assuming
 408 statistical independence). It is clearly seen that the basic result still holds but it is a little less strong (a factor
 409 of ≈ 1.5). The reason for the difference is that the cancellation of the cross terms assumed by statistical

independence is only approximately valid on single realizations, especially at the lower frequencies where the statistics are worse (even on a single realization, at any given scale - except the very longest - there are several fluctuations so that there is still some averaging).

The calculations above ignored the model's internal variability, this was considered small due to the averaging over 100 realizations of the ZC model with the same forcings: the internal is expected to largely cancel out. While it is true that a definitive answer to this requires running the model in "control mode" so as to capture only the internal variability (as was done in for the GISS model, see Fig. 4), there are nevertheless several reasons why the internal variability is almost certainly smaller than the response due to the forcings:

- i) We can get a typical order of magnitude of the internal variability from the GISS model, Fig. 4; we see that for a single realization - without averaging over 100 realizations as in Fig. 3a - that the typical centennial variability is $\approx \pm 0.05\text{K}$ and decreasing with a power law with exponent $\approx \xi(2) / 2 \approx -0.2$. After averaging for 100 realizations, we expect this to decrease by $(100)^{0.5} = 10$, i.e. to $\pm 0.005\text{K}$. This is much smaller than the centennial scale variability of the ZC responses in Fig. 3a (from the graph, these are about $\approx \pm (10^{-1.2}) / 2 \approx \pm 0.03\text{K}$).
- ii) We can use the fact that a) the observed responses are upper bounds on the internal variability and b) that the internal variability must decrease with scale (otherwise the model's climate diverges rather than converges for long times. Exponents near the GISS value $\xi(2) / 2 \approx -0.2$ are common, see e.g. Lovejoy et al., (2013). From Fig. 2, we see that the ZC solar response at ≈ 20 years is $\pm 0.03\text{K}$, so this is an upper bound for the internal variability at all scales longer than ≈ 20 years. However, over the range $\approx 50\text{-}500$ years (relevant for the subadditivity conclusion), the solar response variability is considerably larger than this noise value: from the graph, $\approx \pm (10^{-0.8}) / 2 \approx \pm 0.08\text{K}$.

We conclude that it is unlikely that the internal variability is strong enough to account for the results.

134 In the ZC model, all forcings are input at the surface so that here the subadditivity is due to
135 the differing seasonality, fluctuation intensities and spatial distributions of the solar and volcanic forcings.
136 In the GISS-E2-R GCM simulations, the response to the solar forcing is too small to allow us to determine
137 if it involves a similar solar-volcanic negative feedback (Fig. 4). In GCMs with their vertically stratified
138 atmospheres or the real atmosphere, non additivity is perhaps not surprising given the difference between
139 the solar and volcanic vertical heating profiles. If such negative feedbacks are substantiated in further
140 simulations, it would enhance the credibility of the idea that current GCMs are missing critical slow (multi
141 centennial, multi millennial) climate processes. No matter what the exact explanation, non additivity
142 underlines the limitations of the convenient reduction of climate forcings to radiative forcing equivalents. It
143 also indicates that at scales longer than about 50 yrs energy budget models must nonlinearly account for
144 albedo-temperature interactions (i.e. that linear energy budget models are inadequate at these time scales,
145 and that albedo-temperature interactions must at least be correctly parametrized).

146 Also shown for reference in Fig. 3a are the fluctuations for three multiproxy estimates of annual
147 northern hemisphere temperatures (1500-1900; pre-industrial, Moberg et al., 2005; Huang, 2004;
148 Ljungqvist, 2010, the analysis was taken from Lovejoy and Schertzer, 2012c). Although it should be borne
149 in mind that the ZC model region (the Pacific) does not coincide with the proxy region (the northern
150 hemisphere), the latter is the best model validation available. In addition, since we compare model and
151 proxy fluctuation statistics as functions of time scale, the fact that the spatial regions are somewhat
152 different is less important than if we had attempted a direct year by year comparison of model outputs with
153 the multiproxy reconstructions.

154 In Fig. 3a, we see that the responses of the volcanic only and the combined volcanic and solar
155 forcings fairly well reproduce the RMS multiproxy statistics until ≈ 50 yrs; however at longer time scales,
156 the model fluctuations are substantially too weak – roughly 0.1 K (corresponding to ± 0.05 K) and constant
157 or falling, whereas at 400 yr scales, the RMS multiproxy temperature fluctuations are ≈ 0.25 K (± 0.125)
158 and rising. Indeed, in order to account for the ice ages, they must continue to rise until ≈ 5 K (± 2.5 K) at
159 glacial-interglacial scales of 50 – 100 kyrs, (the “glacial-interglacial window”: according to paleodata, this
160 rise continues in a smooth, power law manner with $H > 0$ until roughly 100 kyrs, see Lovejoy and Schertzer,
161 1986, Shackleton and Imbrie, 1990 Pelletier, 1998, Schmitt et al., 1995, Ashkenazy et al., 2003, Huybers
162 and Curry, 2006, and Lovejoy et al., 2013).

163 In Fig. 4, we compare the RMS Haar fluctuations from the ZC model combined (volcanic and solar
164 forcing) response with those from simulations from the GISS-E2-R GCM with solar only forcing and a
165 control run (no forcings, black; see Lovejoy et al., (2013) for details; the GISS-E2-R solar forcing was the

166 same as the spliced series used in the ZC simulations). We see that the three are remarkably close
 167 over the entire range; for the GISS model, this indicates that the solar only forcing is so small that the
 168 response is nearly the same as for the unforced (control) run. The ZC combined solar and volcanic forcing
 169 is clearly much weaker than the pre-industrial multiproxies (dashed blue, same as in Fig. 3a). The reference
 170 line with slope -0.2 shows the convergence of the control to the model climate; the shallowness of the slope
 171 (-0.2) implies that the convergence is ultra slow. For example, fluctuations from a 10 yr run control run are
 172 only reduced by a factor of $(10 / 3000)^{-0.2} \approx 3$ if the run is extended to 3 kyrs.

173 Finally, in Fig. 5, we compare the responses to the volcanic forcings for the Zebiak-Cane model and
 174 for the GISS-E2-R GCM for two different volcanic reconstructions (Gao et al., 2008), and Crowley, 2000)
 175 (the reconstruction used in the ZC simulation). For reference, we again show the combined ZC response
 176 and the preindustrial multiproxies. We see that the GISS GCM is much more sensitive to the volcanic
 177 forcing than the Zebiak-Cane model; indeed, it is too sensitive at scales $\Delta t \lesssim 100$, but nevertheless becomes
 178 too weak at scales $\Delta t \gtrsim 200$ years. Indeed, since the volcanic forcings continue to decrease with scale, we
 179 expect the responses to keep diminishing with scale at larger Δt .

180 Note that the spatial regions covered by the ZC simulation, the GISS outputs and the multiproxy
 181 reconstructions are not the same. For the latter, the reason is that there is no perfectly appropriate
 182 (regionally defined) multiproxy series whereas for the GISS outputs, we reproduced the structure function
 183 analysis from a published source. Yet, the differences in the regions may not be so important since we are
 184 only making statistical comparisons. This is especially true since all the series are for planetary scale
 185 temperatures (even if they are not identical global sized regions) and in addition, we are mostly interested
 186 in the fifty year (and longer) statistics which may be quite similar.

187 **4. Intermittency: a multifractal trace moment analysis**

188 **4.1 The Trace moment analysis technique**

189 In the previous sections we considered the implications of linearity when climate models were forced
 190 separately with two different forcings compared with the response to the combined forcing; we showed that
 191 the ZC model was subadditive. However, linearity also constrains the relation between the fluctuations in
 192 the forcings and the responses. For example at least since the work of Clement et al., (1996), in the context
 193 of volcanic eruptions, it has been recognized that the models are typically sensitive to weak forcing events
 194 but insensitive to strong ones, i.e. they are nonlinear, and Mann et al., (2005) noticed this in their ZC
 195 simulations.

196 In a scaling regime, both forcings and responses will be characterized by a hierarchy of
 197 exponents (i.e. the function $\xi(q)$ in Eq. 3 or equivalently by the exponent H and the function $K(q)$), the
 198 differences in the statistics of weak and strong events are reflected in these different exponents; high order
 199 moments (large q) are dominated by large fluctuations and conversely for low order moments. The degree
 500 of convexity of $K(q)$ quantifies the degree of these nonlinear effects (indeed, how they vary over time
 501 scales Δt). Such “intermittent” behaviour was first studied in the context of turbulence (Kolmogorov, 1962;
 502 Mandelbrot, 1974).

503 In order to quantify this, recall that if the system is linear, the response is a convolution of the system
 504 Green’s function with the forcing, in spectral terms it acts as a filter. If it is also scaling, then the filter is a
 505 power law: ω^{-H} where ω is the frequency, (mathematically, if $\mathcal{F}(\omega)$ and $\mathcal{F}(\omega)$ are the Fourier transforms of
 506 the response and forcing, for a scaling linear system, we have: $\mathcal{F}(\omega) \propto \omega^{-H} \mathcal{F}(\omega)$ such a filter corresponds to
 507 a fractional integration of order H). In terms of fluctuations this implies: $\Delta T(\Delta t) = \Delta t^H \Delta F(\Delta t)$ (assuming that
 508 the fluctuations are appropriately defined). Therefore, by taking q^{th} powers of both sides and ensemble
 509 averaging, we see that in linear scaling systems we have: $\xi_r(q) = qH + \xi_f(q)$ (c.f. eq. (3) with $\xi_r(q)$ and $\xi_f(q)$
 510 the structure function exponents for the response and the forcing respectively). If $\xi_r(q)$ and $\xi_f(q)$ only
 511 differ by a term linear in q , then $K_T(q) = K_F(q)$, so that if over some regime, we find empirically $K_T(q) \neq K_F(q)$
 512 (i.e. the intermittencies are different), then we may conclude that that the system is nonlinear (note that this
 513 result is independent of whether the linearity is deterministic or only statistical in nature).

514 Let us investigate the nonlinearity of the exponents by returning to Eq. (1), (2) and (3) in more detail.
 515 Up until now we have studied the statistical properties of the forcings and responses using the RMS
 516 fluctuations e.g. we have used the following equation but only for the value $q = 2$:

$$517 \quad \langle \Delta T(\Delta t)^q \rangle \propto \langle \varphi_{\lambda'}^q \rangle \Delta t^{qH} = \Delta t^{\xi(q)}; \quad \xi(q) = qH - K(q) \quad (6)$$

518 (see Eq. (1)) the exponent $K(q)$ (implicitly defined in (3)) is given explicitly by:

$$519 \quad \langle \varphi_{\lambda'}^q \rangle = \Delta t^{K(q)}; \quad \frac{\tau_{eff}}{\Delta t} \quad (7)$$

520 where τ_{eff} is the effective outer scale of the multifractal cascade process, φ gives rise to the strong
 521 variability and λ' is the cascade ratio from this outer scale to the scale of interest Δt .

522 If the driving flux φ was quasi-Gaussian, then $K(q)=0$, $\xi(q) = qH$ and the exponent $\xi(2) = 2H = \beta - 1$
 523 would be sufficient for a complete characterization of the statistics. However geophysical series are often

524 far from Gaussian, even without statistical analysis, a visual inspection (the sharp spike” of
 525 varying amplitudes, see Fig. 1a) of the volcanic series makes it obvious that it is particularly extreme in this
 526 regard. We expect - at least in this case - that the $K(q)$ term will readily be quite large (although note the
 527 constraint $K(1)=0$ and the mean of φ (the $q=1$ statistic) is independent of scale). To characterize this, note
 528 that since $K(1)=0$, we have $\xi(1)=H$ and then use the first two derivatives of $\xi(q)$ at $q=1$ to estimate the
 529 tangent (linear approximation) to $K(q)$ near the mean (C_1) and the curvature of $K(q)$ near the mean
 530 characterized by α . This gives

$$531 \left. \begin{aligned} (C_1) &= K'(1) = H - \xi'(1) \\ \alpha &= K''(1) / K'(1) = \xi''(1) / (\xi'(1) - H) \end{aligned} \right\} \quad (8)$$

532 The parameters C_1, α are particularly convenient since – thanks to a kind of multiplicative central
 533 limit theorem - there exist multifractal universality classes (Schertzer and Lovejoy, 1987). For such
 534 universal multifractal processes, the exponent function $K(q)$ can be entirely (i.e. not only near $q=1$)
 535 characterized by the same two parameters:

$$536 K(q) = \frac{C_1}{\alpha-1} (q^\alpha - q); \quad 0 \leq \alpha \leq 2 \quad (9)$$

537 In the universality case (9), it can be checked that the estimate in (8) (near the mean) is satisfied so
 538 that C_1, α characterize all the statistical moments (actually, (6), (7) are only valid for $q < q_c$; for $q > q_c$,
 539 the above will break down due to multifractal phase transitions; the critical q_c is typically >2 , so that here
 540 we confine our analyses to $q \leq 2$ and do not discuss the corresponding extreme - large q - behaviour).

541 A drawback of the above fluctuation method for using $\xi(q)$ to estimate $K(q)$ (6) is that if C_1 is not
 542 too big, then for the low order moments q , the exponent $\xi(q)$ may be dominated by the linear (qH)
 543 term, so that the multifractal part ($K(q)$) of the scaling is not too apparent. A simple way of directly studying
 544 $K(q)$ is to transform the original series so as to estimate the flux φ at a small scale, essentially removing the
 545 (qH) part of the exponent. It can then be degraded by temporal averaging and the scaling of the various
 546 statistical moments - the exponents $K(q)$ - can be estimated directly. To do this, we divide (1) by its
 547 ensemble average so as to estimate the normalized flux at the highest resolution by:

$$548 \varphi' = \frac{\varphi}{\langle \varphi \rangle} = \frac{\Delta T}{\langle \Delta T \rangle} \quad (10)$$

where the ensemble average (“ $\langle \rangle$ ”) is estimated by averaging over the available data (here a single series), and the fluctuations Δt are estimated at the finest resolution (here 1 yr).

4.2 Trace moment analysis of forcings, responses and multiproxies

We now test (7); for convenience, we use the symbol λ as the ratio of a convenient reference scale – here the length of the series, $\tau_{ref} = 1000$ yrs to the resolution scale Δt (for some analyses, 400 yrs was used instead, see the captions in Fig. 6). In an empirical study, the outer scale τ_{eff} is not known a priori, it must be empirically estimated; denote the scale at which the cascade starts by λ'

Starting with (7), the basic prediction of multiplicative cascades is that the normalized moments ϕ' (10) obey the generic multiscaling relation:

$$M(q) = \langle \phi'_{\lambda^q} \rangle = \lambda'^{K(q)} = \left(\frac{\tau_{eff}}{\Delta t} \right)^{K(q)} = \left(\frac{\lambda}{\lambda_{eff}} \right)^{K(q)} ; \lambda' = \frac{\tau_{eff}}{\Delta t} = \frac{\lambda}{\lambda_{eff}} ; \lambda_{eff} = \frac{\tau_{ref}}{\tau_{eff}} \quad (11)$$

We can see that τ_{eff} can readily be empirically estimated since a plot of $\text{Log}_{10} M$ versus $\text{Log}_{10} \lambda$ will have lines (one for each q , slope $K(q)$) converging at the outer scale $\lambda = \lambda_{eff}$ (although for a single realisation such as here, the outer scale will be poorly estimated since clearly for a single sample (series) there is no variability at the longest time scales, there is a single long-term value that generally poorly represents the ensemble mean). Figure 6a shows the results when ΔT is estimated by the absolute second difference at the finest resolution. The solar forcing (upper right) was only shown for the recent period (1600-2000) over which the higher resolution sunspot based reconstruction was used, the earlier 1000-1600 part was based on a (too) low resolution ^{10}Be “splice” as discussed above, see Fig. 2b. In the solar plot (upper left), but especially in the volcanic forcing plot (upper right), we see that the scaling is excellent over nearly the entire range (the points are nearly linear) and in addition, the lines plausibly “point” (i.e. cross) at a unique outer scale $\lambda = \lambda_{eff}$ which is not far from the length of the series, see Table 1 for estimates of the corresponding time scales. From these plots we see that the responses to the volcanic forcing “spikiness” (intermittency) are much stronger than to the corresponding responses to the weaker solar “spikiness”. The model atmosphere therefore considerably dampens the intermittency, but in addition this effect is highly nonlinear so that the intermittency of the combined volcanic and solar forcing (bottom left) is actually a little less than the volcanic only intermittency (bottom right). Table 1 gives a quantitative characterization of the intermittency strength near the mean, using the C_1 parameter.

578 It is interesting at this stage to compare the intermittency of the ZC outputs with those of the
 579 GISS-E2-R GCM (Fig. 6b) and with multiproxy temperature reconstructions (Fig. 6c). In Fig. 6b, we see
 580 that the GISS-E2-R trace moments rapidly die off at large scales (small λ) so that the intermittency is
 581 limited to small scales to the right of the convergence point. In this Figure, we see that the lines converge at
 582 $\text{Log}_{10}\lambda \approx 1.1-1.5$ corresponding to τ_{eff} in the range roughly 10–30 yrs. Since the intermittency builds up
 583 scale by scale from large scales modulating smaller scales in a hierarchical manner, and since this range of
 584 scales is small, the intermittency will be small. The partial exception is for the upper right plot which is for
 585 the GISS-E2-R response to the large Gao volcanic forcing (recall that the ZC model uses the weaker,
 586 Crowley volcanic reconstruction whose response is strongly intermittent, see Fig. 6b, the upper left plot).
 587 This result shows that contrary to the ZC model whose response is strongly intermittent (highly non
 588 Gaussian) over most of the range of time scales, the GISS-E2-R response is nearly Gaussian implying that
 589 the (highly non Gaussian) forcings are quite heavily (nonlinearly) damped.

590 This difference in the model responses to the forcing intermittency is already interesting, but it does
 591 not settle the question as to which model is more realistic. To attempt to answer this question, we turn to
 592 Fig. 6c which shows the trace moment analysis for six multiproxy temperature reconstructions over the
 593 same (pre-industrial) period as the GISS-E2-R model (1500-1900; unlike the ZC model, the GISS-E2-R
 594 included anthropogenic forcings so that the period since 1900 was not used in the GISS-E2-R analysis).
 595 Statistical comparisons of nine multiproxies were made in ch. 11 of Lovejoy and Schertzer, (2013), (for
 596 reasons of space, only six of these are shown in Fig. 6c) where it was found that the pre 2003 multiproxies
 597 had significantly smaller multicentennial and lower frequency variability than the more recent multiproxies
 598 used as reference in Fig. 4 and 5. However, Fig. 6c shows that the intermittencies are all quite low (with the
 599 partial exception of the Mann series, see the upper right plot). This conclusion is supported by the
 500 comparison with the red curves. These indicate the generic envelope of trace moments of quasi-Gaussian
 501 processes for $q \leq 2$ it shows how the latter converge (at large scales, small λ , to the left) to the flat
 502 ($K(q) = 0$) Gaussian limit. We see that the actual lines are only slightly outside this envelope showing that
 503 they are only marginally more variable than quasi-Gaussian processes.

504 The comparison of the GISS-E2-R outputs (Fig. 6b) with the multiproxies (Fig. 6c) indicates that
 505 they are both of low intermittency and are more similar to each other than to the ZC multiproxy statistics.
 506 One is therefore tempted to conclude that the GISS-E2-R model is more realistic than the ZC model with
 507 its much stronger intermittency. However this conclusion may be premature since the low multiproxy and
 508 GISS intermittencies may be due to limitations of both the multiproxies and the GISS-E2-R model.

509 Multicentennial and multimillennial scale ice core analyses displays significant paleotemperature
510 intermittency ($C_1 \approx 0.05-0.1$, Schmitt et al., 1995 see the discussion in ch. 11 of Lovejoy and Schertzer, 2013)
511 so that the multiproxies may be insufficiently intermittent.

512 **5. Conclusions**

513 From the point of view of GCM's, climate change is a consequence of changing boundary conditions
514 (including composition), the latter are the climate forcings. Since forcings of interest (such as
515 anthropogenic forcings) are typically of the order of 1% of the mean solar input the responses are plausibly
516 linear. This justifies the reduction of the forcings to a convenient common denominator: the “equivalent
517 radiative forcing”, a concept which is useful only if different forcings add linearly, if they are “additive”.
518 An additional consequence of linearity is that the climate sensitivities are independent of whether the
519 fluctuations in the forcings are weak or strong. Both consequences of linearity clearly have their limits. For
520 example, at millennial and longer scales, energy balance models commonly discard linearity altogether and
521 assume that nonlinear albedo responses to orbital changes are dominant. Similarly, at monthly and annual
522 scales, the linearity of the climate sensitivity has been questioned in the context of sharp, strong volcanic
523 forcings.

524 In view of the widespread use of the linearity assumption, it is important to quantitatively establish its
525 limits and this can best be done using numerical climate models. A particularly convenient context is
526 provided by the Last Millennium simulations, which (in the preindustrial epoch) are primarily driven by the
527 physically distinct solar and volcanic forcings (forcings due to land use changes are very weak). The ideal
528 would be to have a suite of the responses of fully coupled GCM's which include solar only, volcanic only
529 and combined solar and volcanic forcings and control runs (for the internal variability) so that the responses
530 could be evaluated both individually and when combined. Unfortunately, the optimal set of GCM products
531 are the GISS E2-R millennium simulations with solar only and solar plus volcanic forcing and a control run
532 (this suite is missing the volcanic only responses). We therefore also considered the outputs of a simplified
533 climate model, the Zebiac-Cane (ZC) model (Mann et al., 2005) for which the full suite of external forcing
534 response was available.

535 Following a previous study, we first quantified the variability of the forcings as a function of time
536 scale by considering fluctuations. These were estimated by using the difference between the averages of the
537 first and second halves of intervals Δt (“Haar” fluctuations). This definition was necessary in order to
538 capture the two qualitatively different regimes, namely those in which the average fluctuations increase

539 with time scale ($H > 0$) and those in which they decrease with scale ($H < 0$). Whereas the solar
 540 forcing was small at annual scales, it generally increased with scale. In comparison, the volcanic forcing
 541 was very strong at annual scales but rapidly decreased, the two becoming roughly equal at about 200 yrs.
 542 By considering the response to the combined forcing we were then able to examine and quantify their non-
 543 additivity (nonlinearity). By direct analysis (Fig. 3b, c), it was found that in the ZC model, additivity of the
 544 radiative forcings only works up until roughly 50 yr scales; at 400 yr scales, there are negative feedback
 545 interactions between the solar and volcanic forcings that reduce the combined effect by a factor of $\approx 1.5 - 2$.
 546 This “subadditivity” makes their combined effects particularly weak at these scales. Although this result
 547 seems statistically robust for the ZC Millenium simulations, until the source of the nonlinearity is pin-
 548 pointed and the results reproduced with full-blown coupled GCM’s, they must be considered tentative (the
 549 conclusions would also be strengthened if ZC control runs output were available to estimate the internal
 550 variability), many more simulations with diverse forcings are needed to completely settle the issue..

551 In order to investigate possible nonlinear responses to sharp, strong events (such as volcanic
 552 eruptions), we used the fact that if the system is linear and scaling, then the difference between the structure
 553 function exponents ($\xi(q)$) for the forcings and responses is itself a linear function of the order of moment q
 554 (moments with large q are mostly sensitive to the rare large values, small q moments are dominated by the
 555 frequent low values). By using the trace moment analysis technique, we isolated the nonlinear part of $\xi(q)$
 556 (i.e. the function $K(q)$) which quantifies the intermittent (multifractal, highly non-Gaussian) part of the
 557 variability (associated with the “spikiness” of the signal). Unsurprisingly we showed that the volcanic
 558 intermittency was much stronger than the solar intermittency, but that in both cases, the model responses
 559 were highly smoothed, they were practically nonintermittent (close to Gaussian) hence that the model
 560 responses to sharp, strong events were not characterized by the same sensitivity as to the more common
 561 weaker forcing events.

562 By examining model outputs, we have found evidence that the response of the climate system is
 563 reasonably linear with respect to the forcing up to time scales of 50 yrs at least for weak (i.e. not sharp,
 564 intermittent) events. But the sharp, intermittent events such as volcanic eruptions that occasionally disrupt
 565 the linearity at shorter time scales, become rapidly weaker at longer and longer time scales (with scaling
 566 exponent $H \approx -0.3$). In practice, linear stochastic models may therefore be valid from over most of the
 567 macroweather range, from ≈ 10 days to over 50 years. However, given their potential importance, it would
 568 be worth designing specific coupled climate model experiments in order to investigate this further.

569

570 **6. Acknowledgements:**

571 The ZC simulation outputs and corresponding solar and volcanic forcings were taken from
 572 ftp://ftp.ncdc.noaa.gov/pub/data/paleo/climate_forcing/mann2005/mann2005.txt. We thank J. Lean (solar
 573 data Fig. 2b (top), Judith.Lean@nrl.navy.mil), A. Shapiro (solar data, Fig. 2b (bottom) Alexander Shapiro,
 574 alexander.shapiro@pmodwrc.ch) and G. Schmidt (the GISS-E2-R simulation outputs,
 575 gavin.a.schmidt@nasa.gov) for graciously providing data and model outputs. The ECHAM5 based
 576 Millenium simulations analyzed in table 1 were available from: [https://www.dkrz.de/Klimaforschung-
 577 en/konsortial-en/millennium-experiments-1?set_language=en](https://www.dkrz.de/Klimaforschung-en/konsortial-en/millennium-experiments-1?set_language=en). Mathematica and MatLab codes for
 578 performing the Haar fluctuation analyses are available from:
 579 <http://www.physics.mcgill.ca/~gang/software/index.html>. This work was unfunded, there were no conflicts
 580 of interest.

581 **References**

- 582 Anderson, J. L.: A method for producing and evaluating probabilistic forecasts from ensemble model
 583 integrations, *J. Climate*, 9, 1518–1530, 1996.
- 584 Ashkenazy, Y., D. Baker, H. Gildor, and Havlin, S.: Nonlinearity and multifractality of climate change in
 585 the past 420,000 years, *Geophys. Res. Lett.*, 30, 2146 doi: 10.1029/2003GL018099, 2003
- 586 Blender, R., and Fraedrich, K.: Comment on “Volcanic forcing improves atmosphere–ocean coupled
 587 general circulation model scaling performance” by D. Vyushin, I. Zhidkov, S. Havlin, A. Bunde, and
 588 S. Brenner, *Geophys. Res. Lett.*, 31, L22213, doi: 10.1029/2004GL020797, 2004.
- 589 Bothe, O., Jungclaus, J. H., and Zanchettin, D.: Consistency of the multi-model CMIP5/PMIP3-past1000
 590 ensemble, *Climate of the Past*, 9 (6), 2471-2487, 2013a.
- 591 Bothe, O., Jungclaus, J. H., Zanchettin, D., and Zorita, E.: Climate of the last millennium: Ensemble
 592 consistency of simulations and reconstructions, *Climate of the Past*, 9 (3), 1089-1110, 2013b.
- 593 Bryson, R. A.: The Paradigm of Climatology: An Essay, *Bull. Amer. Meteor. Soc.*, 78, 450-456, 1997.
- 594 Budyko, M. I.: The effect of solar radiation variations on the climate of the earth, *Tellus*, 21, 611-619, 1969.
- 595 Bunde, A., Eichner, J. F., Kantelhardt, J. W, and Havlin, S.: Long-term memory: a natural mechanism for
 596 the clustering of extreme events and anomalous residual times in climate records, *Phys. Rev. Lett.* ,
 597 94, 1-4 doi: 10.1103/PhysRevLett.94.048701, 2005.

- 598 Chandra, S., Varotsos, C., and Flynn, L. E. The mid-latitude total ozone trends in the northern
599 hemisphere, *Geophys Res Lett.*, 23(5), 555-558, 1996.
- 700 Clement, A. C., Seager, R., Cane, M. A., and Zebiak, S. E.: An ocean dynamical thermostat, 2190–2196,
701 1996.
- 702 Cracknell, A. P., and Varotsos, C. A.: New aspects of global climate-dynamics research and remote sensing.
703 *Int. J. Remote Sens.*, 32(3), 579-600, 2011.
- 704 Cracknell, A. P., & Varotsos, C. A.: The Antarctic 2006 ozone hole. *Int. J. Remote Sens.*, 28(1), 1-2, 2007.
- 705 Crowley, T. J. :Causes of Climate Change Over the Past 1000 Years, *Science*, 289, 270 doi:
706 10.1126/science.289.5477.270, 2000.
- 707 Dijkstra, H.: *Nonlinear Climate Dynamics*, 357 pp., Cambridge University Press, Cambridge, 2013.
- 708 Efstathiou, M. N., Tzani, C., Cracknell, A. P., and Varotsos, C. A.: New features of land and sea surface
709 temperature anomalies. *Int. J. Remote Sens.*, 32(11), 3231-3238, 2011.
- 710 Eichner, J. F., Koscielny-Bunde, E., Bunde, A., Havlin, S., and Schellnhuber, H.-J.: Power-law persistence
711 and trends in the atmosphere: A detailed study of long temperature records, *Phys. Rev. E*, 68,
712 046133-046131-046135 doi: 10.1103/PhysRevE.68.046133, 2003.
- 713 Fraedrich, K., Blender, R., and Zhu, X.: Continuum Climate Variability: Long-Term Memory, Scaling, and
714 1/f-Noise, *International Journal of Modern Physics B*, 23, 5403-5416, 2009.,
- 715 Franzke, J., Frank, D., Raible, C. C., Esper, J., and Brönnimann, S.: Spectral biases in tree-ring climate
716 proxies *Nature Clim. Change*, 3, 360-364 doi: doi: 10.1038/Nclimate1816, 2013.
- 717 Fredriksen, H.-B., and Rypdal, K.: Scaling of Atmosphere and Ocean Temperature Correlations in
718 Observations and Climate Models, *J. Climate* doi: doi.org/10.1175/JCLI-D-15-0457.1, 2015.
- 719 Gao, C. G., Robock, A., and Ammann, C.: Volcanic forcing of climate over the past 1500 years: and
720 improved ice core-based index for climate models, *J. Geophys. Res.*, 113, D23111 doi:
721 10.1029/2008JD010239, 2008.
- 722 Goswami, B. N., and Shukla, J.: Aperiodic Variability in the Cane—Zebiak Model, *J. of Climate*, 6, 628-
723 638, 1991.
- 724 Hansen, J., Sato, M. K. I., Ruedy, R., Nazarenko, L., Lacis, A., Schmidt, G. A., and Bell, N.: Efficacy of
725 climate forcings, *J. Geophys. Res.*, 110, D18104 doi:10.1029/2005JD005776, 2005.
- 726 Hasselmann, K.: Stochastic Climate models, part I: Theory, *Tellus*, 28, 473-485, 1976
- 727 Huang, S.: Merging Information from Different Resources for New Insights into Climate Change in the
728 Past and Future, *Geophys. Res. Lett.*, 31, L13205 doi:10.1029/2004 GL019781, 2004.
- 729 Hurst, H. E.: Long-term storage capacity of reservoirs, *Trans. Amer. Soc. Civil Eng.*, 116, 770-808, 1951.

- 730 Huybers, P., and Curry, W.: Links between annual, Milankovitch and continuum temperature
731 variability, *Nature*, 441, 329-332 doi:10.1038/nature04745, 2006.
- 732 Kantelhardt, J. W., Koscielny-Bunde, E., Rybski, D., Braun, P., Bunde, A., and Havlin, S.: Long-term
733 persistence and multifractality of precipitation and river runoff record, *J. Geophys. Res.*, 111 doi:
734 doi:10.1029/2005JD005881, 2006.
- 735 Kolesnikov, V. N., and Monin, A. S.: Spectra of meteorological field fluctuations, *Izvestiya, Atmospheric
736 and Oceanic Physics*, 1, 653-669, 1965.,
- 737 Kolmogorov, A. N.: A refinement of previous hypotheses concerning the local structure of turbulence in
738 viscous incompressible fluid at high Reynolds number, *Journal of Fluid Mechanics*, 83, 349, 1962,
- 739 Kondratyev, K. Y., and Varotsos, C. A.: Volcanic eruptions and global ozone dynamics, *Int. J. Remote
740 Sens.*, 16 (10), 1887-1895, 1995a.
- 741 Kondratyev, K. Y., and Varotsos, C. A.: Atmospheric greenhouse - effect in the context of global climate-
742 change *NUOVO CIMENTO DELLA SOCIETA ITALIANA DI FISICA C-GEOPHYSICS AND
743 SPACE PHYSICS* 18, 123-151, 1995b
- 744 Koscielny-Bunde, E., Bunde, A., Havlin, S., Roman, H. E., Goldreich, Y., and Schellnhuber, H. J.:
745 Indication of a universal persistence law governing atmospheric variability, *Phys. Rev. Lett.* , 81,
746 729-732, 1998.
- 747 Krivova, N. A., Balmaceda, L., and Solanski, S. K.: Reconstruction of solar total irradiance since 1700
748 from the surface magnetic field flux, *Astron. and Astrophys*, 467, 335-346 doi: 10.1051/0004-
749 6361:20066725, 2007.
- 750 Laepple, T., Jewson, S., and Coughlin, K.: Interannual temperature predictions using the CMIP3 multi-
751 model ensemble mean, *Geophys. Res. Lett.*, 35, L10701, doi:10.1029/2008GL033576, 2008.
- 752 Lean, J. L.: Evolution of the Sun's Spectral Irradiance Since the Maunder Minimum, *Geophys. Res Lett.*, 27,
753 2425-2428, 2000.
- 754 Lean, J. L., and Rind, D. H.: How natural and anthropogenic influences alter global and regional surface
755 temperatures: 1889 to 2006, *Geophys. Res. Lett.*, 35, L18701 doi: 10.1029/2008GL034864, 2008.
- 756 Ljungqvist, F. C.: A new reconstruction of temperature variability in the extra - tropical Northern
757 Hemisphere during the last two millennia, *Geografiska Annaler: Physical Geography*, 92 A(3), 339 -
758 351 doi:10.1111/j .1468 - 0459.2010 .00399.x, 2010.
- 759 Lovejoy, S.: What is climate?, *EOS*, 94, (1), 1 January, p1-2, 2013.
- 760 Lovejoy, S.: Scaling fluctuation analysis and statistical hypothesis testing of anthropogenic warming,
761 *Climate Dyn.*, 42, 2339-2351 doi:10.1007/s00382-014-2128-2, 2014a.

- 762 Lovejoy, S.: A voyage through scales, a missing quadrillion and why the climate is not what ou
763 expect, *Climate Dyn.*, 44, 3187-3210, doi: 10.1007/s00382-014-2324-0, 2014b.,
- 764 Lovejoy, S.: The macroweather to climate transition in the Holocene: regional and epoch to epoch
765 variability (comments on “Are there multiple scaling regimes in Holocene temperature records?” by T.
766 Nilsen, K. Rypdal, and H.-B. Fredriksen), *Earth Syst. Dynam. Discus.*, 6, C1–C10, 2015a.
- 767 Lovejoy, S.: Using scaling for macroweather forecasting including the pause, *Geophys. Res. Lett.*, 42,
768 7148–7155 doi:10.1002/2015GL065665, 2015b.
- 769 Lovejoy, S., and Schertzer, D.: Scale invariance in climatological temperatures and the local spectral
770 plateau, *Annales Geophysicae*, 4B, 401-410, 1986.,
- 771 Lovejoy, S., and Schertzer, D.: Towards a new synthesis for atmospheric dynamics: space-time cascades,
772 *Atmos. Res.*, 96, 1-52 doi:10.1016/j.atmosres.2010.01.004, 2010.
- 773 Lovejoy, S., and Schertzer, D.: Stochastic and scaling climate sensitivities: solar, volcanic and orbital
774 forcings, *Geophys. Res. Lett.*, 39, L11702, doi:10.1029/2012GL051871, 2012a.,
- 775 Lovejoy, S., and Schertzer, D.: Low frequency weather and the emergence of the Climate, in *Extreme*
776 *Events and Natural Hazards: The Complexity Perspective*, edited by A. S. Sharma, A. Bunde, D. N.
777 Baker and V. P. Dimri, pp. 231-254, AGU monographs, Washington D.C., 2012b,
- 778 Lovejoy, S., and Schertzer, D.: Haar wavelets, fluctuations and structure functions: convenient choices for
779 geophysics, *Nonlinear Proc. Geophys.*, 19, 1-14, doi:10.5194/npg-19-1-2012, 2012c.
- 780 Lovejoy, S., and Schertzer, D.: *The Weather and Climate: Emergent Laws and Multifractal Cascades*, 496
781 pp., Cambridge University Press, Cambridge, 2013.
- 782 Lovejoy, S., Schertzer, D., and Varon, D.: Do GCM’s predict the climate.... or macroweather?, *Earth Syst.*
783 *Dynam.*, 4, 1–16 doi:10.5194/esd-4-1-2013, 2013.,
- 784 Lovejoy, S., Muller, J. P., and Boisvert, J. P.: On Mars too, expect macroweather, *Geophys. Res. Lett.*,
785 41, 7694-7700, doi:10.1002/2014GL061861, 2014.
- 786 Lovejoy, S., del Rio Amador, L., and Hébert, R.: The ScaLIing Macroweather Model (SLIMM): using
787 scaling to forecast global-scale macroweather from months to Decades, *Earth Syst. Dynam.*, 6, 1–22,
788 <http://www.earth-syst-dynam.net/6/1/2015/>, doi:10.5194/esd-6-1-2015, 2015.
- 789 Mandelbrot, B. B.: Intermittent turbulence in self-similar cascades: divergence of high moments and
790 dimension of the carrier, *Journal of Fluid Mechanics*, 62, 331-350, 1974.
- 791 Mann, M. E., Cane, M. A., Zebiak, S. E., and Clement, A.: Volcanic and solar forcing of the tropical
792 pacific over the past 1000 years, *J. Clim.*, 18, 447-456, 2005.

- 793 Marzban, C., Wang, R., Kong, F., and Leyton, S.: On the effect of correlations on rank histograms:
 794 reliability of temperature and wind speed forecasts from fine scale ensemble reforecasts, *Mon.*
 795 *Weather Rev.*, 139, 295–310, doi:doi:10.1175/2010MWR3129.1, 2011.
- 796 Meehl, G. A., Washington, W. M., Ammann, C. M., Arblaster, J. M., Wigley, T. M. L., and Tebaldi, C.:
 797 Combinations Of Natural and Anthropogenic Forcings In Twentieth-Century Climate, *J. of Clim.*,
 798 17, 3721-3727, 2004.
- 799 Miller, G. H., Geirsdóttir, Á., Zhong, Y., Larsen, D. J., Otto Bliesner, B. L., Holland, M. M., and Anderson,
 300 C.: Abrupt onset of the Little Ice Age triggered by volcanism and sustained by sea-ice/ocean
 301 feedbacks, *Geophys. Res. Lett.*, 39, L02708 doi:10.1029/2011GL050168, 2012.
- 302 Minnis, P., Harrison, E. F., Stowe, L. L., Gibson, G. G., Denn, F. M., Doelling, D. R., and Smith Jr, W. L.:
 303 Radiative Climate Forcing by the Mount Pinatubo Eruption, *Science*, 259 (5100), 1411-1415, 1993.
- 304 Moberg, A., Sonnechkin, D. M., Holmgren, K., Datsenko, N. M., and Karlén, W.: Highly variable Northern
 305 Hemisphere temperatures reconstructed from low- and high - resolution proxy data, *Nature*,
 306 433(7026), 613-617, 2005.
- 307 Newman, M.: An Empirical Benchmark for Decadal Forecasts of Global Surface Temperature Anomalies,
 308 *J. of Clim.*, 26, 5260-5269, doi:10.1175/JCLI-D-12-00590.1, 2013.
- 309 Newman, M. P., Sardeshmukh, P. D., and Whitaker, J. S.: A study of subseasonal predictability, *Mon.*
 310 *Wea. Rev.*, 131, 1715-1732, 2003.
- 311 Nicolis, C.: Transient climatic response to increasing CO₂ concentration: some dynamical scenarios, *Tellus*
 312 *A*, 40A, 50-60, doi:10.1111/j.1600-0870.1988.tb00330.x, 1988.
- 313 Østvand, L., Nilsen, T., Rypdal, K., Divine, D., and Rypdal, M.: Long-range memory in millennium-long
 314 ESM and AOGCM experiments, *Earth System Dynamics*, 5, ISSN 2190-4979.s 2295 - 2308.s,
 315 doi:10.5194/esd-5-295-2014, 2014.
- 316 Panofsky, H. A., and Van der Hoven, I.: Spectra and cross-spectra of velocity components in the
 317 mesometeorological range, *Quarterly J. of the Royal Meteorol. Soc.*, 81, 603-606, 1955.
- 318 Pelletier, J., D.: The power spectral density of atmospheric temperature from scales of 10⁻² to 10⁶ yr, *EPSL*,
 319 158, 157-164, 1998.
- 320 Peng, C.-K., Buldyrev, S. V., Havlin, S., Simons, M., Stanley, H. E., and Goldberger, A. L.: Mosaic
 321 organisation of DNA nucleotides, *Phys. Rev. E*, 49, 1685-1689, 1994.,
- 322 Penland, C., and Sardeshmukh, P. D.: The optimal growth of tropical sea surface temperature anomalies, *J.*
 323 *Climate*, 8, 1999-2024, 1995.

- 324 Pielke, R.: Climate prediction as an initial value problem, *Bull. of the Amer. Meteor. Soc.*, 79,
325 2743-2746, 1998.
- 326 Ragone, F., Lucarini, V., and Lunkeit, F.: A new framework for climate sensitivity and prediction: a
327 modelling perspective, *Climate Dynamics*, 1-13, 2014.
- 328 Roques, L., Chekroun, M. D., Cristofol, M., Soubeyrand, S., and Ghi, M.: Parameter estimation for energy
329 balance models with memory, *Proc. Roy. Soc. A*, 470 20140349 doi: DOI: 10.1098/rspa.2014.0349,
330 2014.
- 331 Rybski, D., Bunde, A. Havlin, S., and von Storch, H.: Long-term persistence in climate and the detection
332 problem, *Geophys. Resear. Lett.*, 33, L06718-06711-06714, doi:10.1029/2005GL025591, 2006.
- 333 Rypdal, M., and Rypdal, K.: Long-memory effects in linear response models of Earth's temperature and
334 implications for future global warming, *J. Climate*, 27 (14), 5240 - 5258, doi:10.1175/JCLI-D-13-
335 00296.1, 2014.
- 336 Sardeshmukh, P. D., and Sura, P.: Reconciling non-gaussian climate statistics with linear dynamics, *J. of*
337 *Climate*, 22, 1193-1207, 2009.
- 338 Schertzer, D., and Lovejoy, S.: Physical modeling and Analysis of Rain and Clouds by Anisotropic Scaling
339 of Multiplicative Processes, *J Geophys Res*, 92, 9693-9714, 1987.
- 340 Schmidt, G. A., et al.: Using paleo-climate model/data comparisons to constrain future projections in
341 CMIP5, *Clim. Past Discuss.*, 9, 775-835, doi:10.5194/cpd-9-775-2013, 2013.
- 342 Schmitt, F., Lovejoy, S., and Schertzer, D.: Multifractal analysis of the Greenland Ice-core project climate
343 data., *Geophys. Res. Lett.*, 22, 1689-1692, 1995.
- 344 Shackleton, N. J., and Imbrie, J.: The $\delta^{18}O$ spectrum of oceanic deep water over a five-decade band,
345 *Climatic Change*, 16, 217-230, 1990.
- 346 Shapiro, A. I., Schmutz, W., Rozanov, E., Schoell, M., Haberreiter, M., Shapiro, A. V., and Nyeki, S.: A
347 new approach to long-term reconstruction of the solar irradiance leads to large historical solar forcing,
348 *Astronomy & Astrophysics*, 529, A67, doi: doi.org/10.1051/0004-6361/201016173, 2011.
- 349 Shindell, D. T., Schmidt, G. A., Miller, R. I., and Mann, M. E.: Volcanic and Solar Forcing of Climate
350 Change during the Preindustrial Era, *J. Clim.*, 16, 4094-4107, 2003.
- 351 Steinhilber, F., Beer, J., and Frohlich, C.: Total solar irradiance during the Holocene, *Geophys. Res. Lett.*,
352 36, L19704, doi:10.1029/2009GL040142, 2009.
- 353 Van der Hoven, I.: Power spectrum of horizontal wind speed in the frequency range from 0.0007 to 900
354 cycles per hour, *Journal of Meteorology*, 14, 160-164, 1957.

- 355 Varotsos, C. A.: The global signature of the ENSO and SST-like fields. *Theor. Applied Clim.*,
 356 113(1-2), 197-204, 2013.
- 357 Varotsos, C., Efstathiou, M., and Tzanis, C.: Scaling behaviour of the global tropopause. *Atmos Chem*
 358 *Phys*, 9(2), 677-683, 2009.
- 359 Varotsos, C., Kalabokas, P., and Chronopoulos, G.: Association of the laminated vertical ozone structure
 360 with the lower-stratospheric circulation. *J. Applied Meteorol*, 33(4), 473-476, 1994.
- 361 Vyushin, D., Zhidkov, I., Havlin, S., Bunde, A., and Brenner, S.: Volcanic forcing improves atmosphere-
 362 ocean coupled, general circulation model scaling performance. *Geophys. Res. Lett.*, 31, L10206,
 363 doi:10.1029/2004GL019499, 2004.
- 364 Wang, Y.-M., Lean, J. L., and Sheeley, N. R. J.: Modeling the Sun's magnetic field and irradiance since
 365 1713, *Astrophys J.*, 625, 522–538, 2005.
- 366 Watson, A. J. and Lovelock, J. E.: Biological homeostasis of the global environment: the parable of
 367 Daisyworld, *Tellus*, 35B, 284-289, 1983.
- 368 Weber, S. L.: A timescale analysis of the Northern Hemisphere temperature response to volcanic and solar
 369 forcing, *Climate of the Past*, 1, 9–17, 2005.
- 370 Zanchettin, D., Rubino, A., and Jungclaus, J. H.: Intermittent multidecadal-to-centennial fluctuations
 371 dominate global temperature evolution over the last millennium, *Geophys. Res. Lett.*, 37 (14),
 372 L14702, 2010.
- 373 Zanchettin, D., Rubino, A., Matei, D., Bothe, O., and Jungclaus, J. H.: Multidecadal-to-centennial SST
 374 variability in the MPI-ESM simulation ensemble for the last millennium, *Climate Dynamics*, 40 (5-6),
 375 1301-1318, 2013.
- 376 Zebiak, S. E., and Cane, M. A.: A Model El Niño – Southern Oscillation, *Mon. Wea. Rev.*, 115, 2262–2278,
 377 1987. .
- 378 Zhu, X., Fraederich, L., and Blender, R.: Variability regimes of simulated Atlantic MOC, *Geophys. Res.*
 379 *Lett.*, 33, L21603, doi:10.1029/2006GL027291, 2006.

380

381

Tables:

382 **Table 1.** The scaling exponent estimates for the forcings and ZC model responses.

	Forcings		Responses			Control Runs	
	Solar	Volcanic	Solar	Volcanic	Combined	GISS	ECHAM5
H	0.40	-0.21	0.031	-0.17	-0.15	-0.26	-0.4
C_1	0.095	0.48	0.022	0.054	0.038	<0.01	<0.01
α	1.04	0.31	1.82	2.0	2.0	–	–
$\xi(2)/2$	0.33	-0.47	-0.01	-0.28	-0.23	<0.01	<0.01
β	1.66	0.06	0.98	0.44	0.54	0.47	0.2
τ_{eff}	630 yrs	300yrs	100yrs	100 yrs	250 yrs	–	–

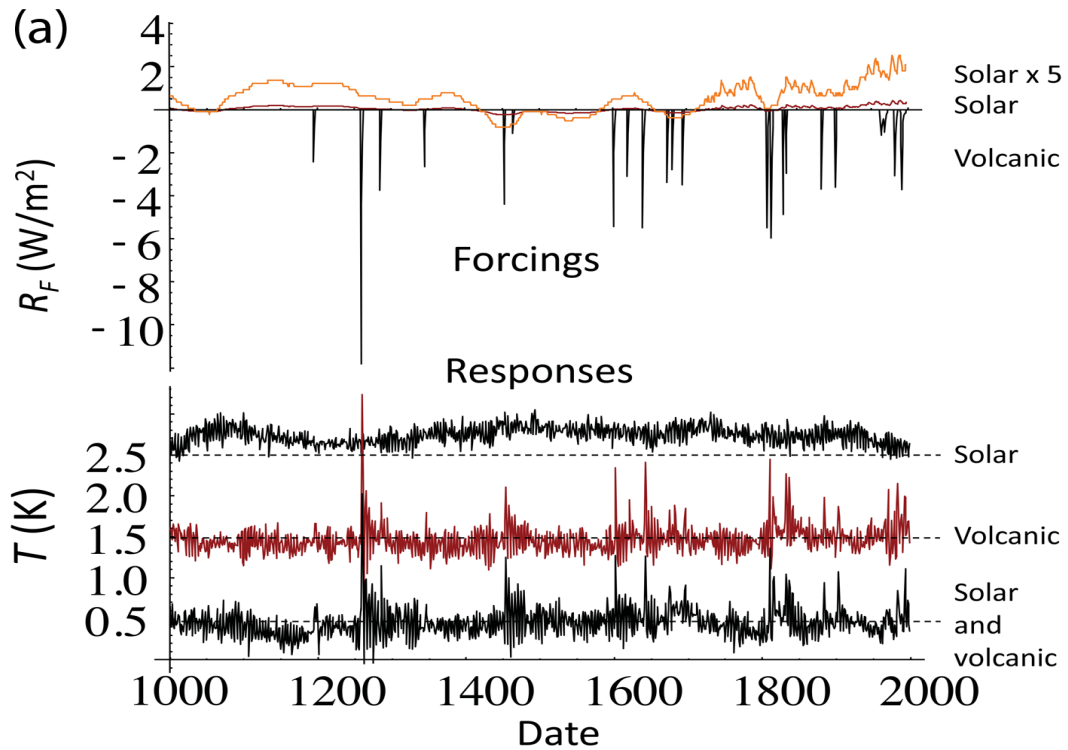
383

384 Table 1 shows the scaling exponent estimates for the forcings and ZC model responses. For the solar
385 (forcing and response), only the recent 400 yrs (sunspot based) series were used, for the others, the entire
386 1000 yrs range was used, see figure 6a. The RMS exponent was estimated from Eq. (6), (9): H was
387 estimated from the Haar fluctuations, α , C_1 were estimated from the trace moments (Fig. 6a). Note that
388 the external cascade scales are unreliable since they were estimated from a single realization. The control
389 runs at the right are for the GISS-E2-R model discussed in the text and (ECHAM5) from the fully coupled
390 COSMOS-ASOB Millenium long term simulations based on the Hamburg ECHAM5 model for 800–
391 4000AD.

392

393

Figures and Captions:



394

395 **Figure 1a.** *Top graph:* The radiative forcings R_F (top, W/m²) and responses T (K) from 1000-2000 AD for
 396 the Zebiak–Cane model, from Mann et al., (2005), integrated over the entire simulation region. The
 397 forcings are reconstructed solar (brown), solar blown up by a factor 5 (orange) and volcanic (red). For the
 398 solar forcing (top series), note the higher resolution and wandering character for the recent centuries – this
 399 part is based on sunspots, not ¹⁰Be.

400 *Bottom graph:* The responses are for the solar forcing only (top), volcanic forcing only (middle) and both
 401 (bottom); they have been offset in the vertical for clarity by 2.5, 1.5, 0.5K, respectively.

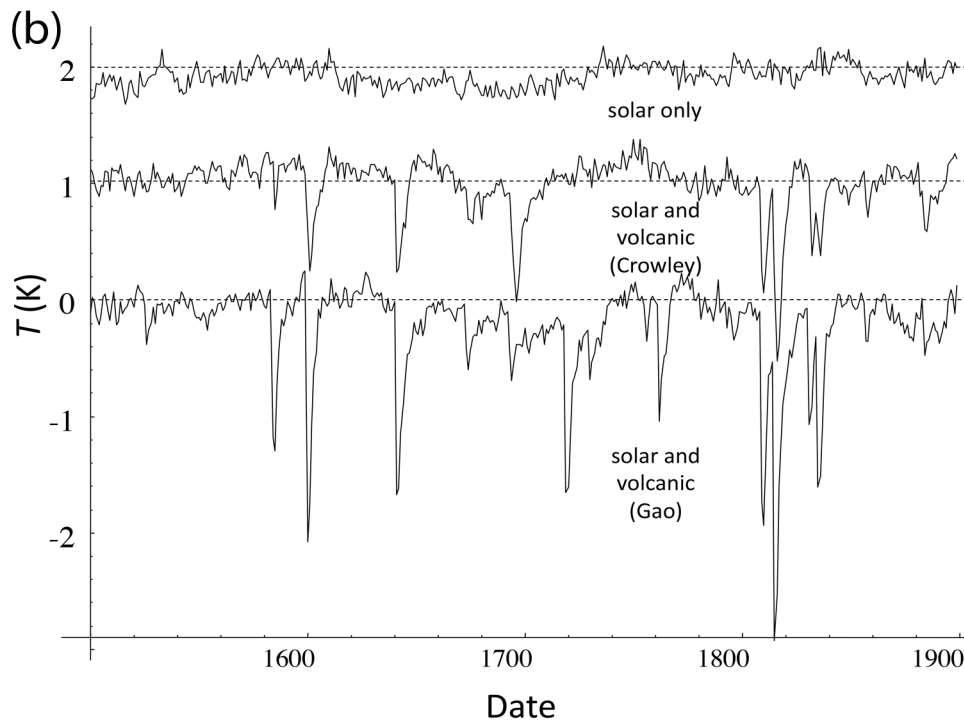
402

403

404

405

406

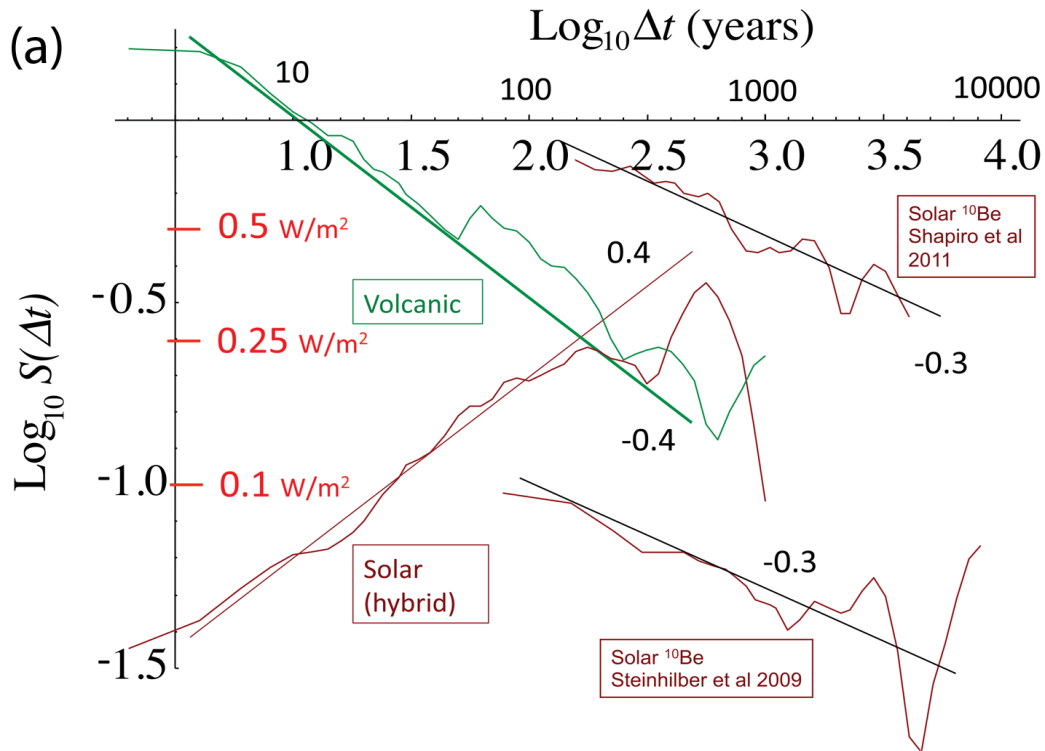


007

008 **Figure 1b.** GISS-ER-2 responses averaged over land, the northern hemisphere at annual resolution. The
 009 industrial part since 1900 was excluded due to the dominance of the anthropogenic forcings. The solar
 010 forcing is the same as for the ZC model, it is mostly sunspot based (since 1610). The top row is for the
 011 solar forcing only, the middle series is the response to the solar and Crowley reconstructed volcanic forcing
 012 series (i.e. the same as used in the ZC model); the bottom series uses the solar and reconstructed volcanic
 013 forcing series from Gao et al., (2008). Each series has been offset in the vertical by 1K for clarity (these are
 014 anomalies so that the absolute temperature values are unimportant).

015

016

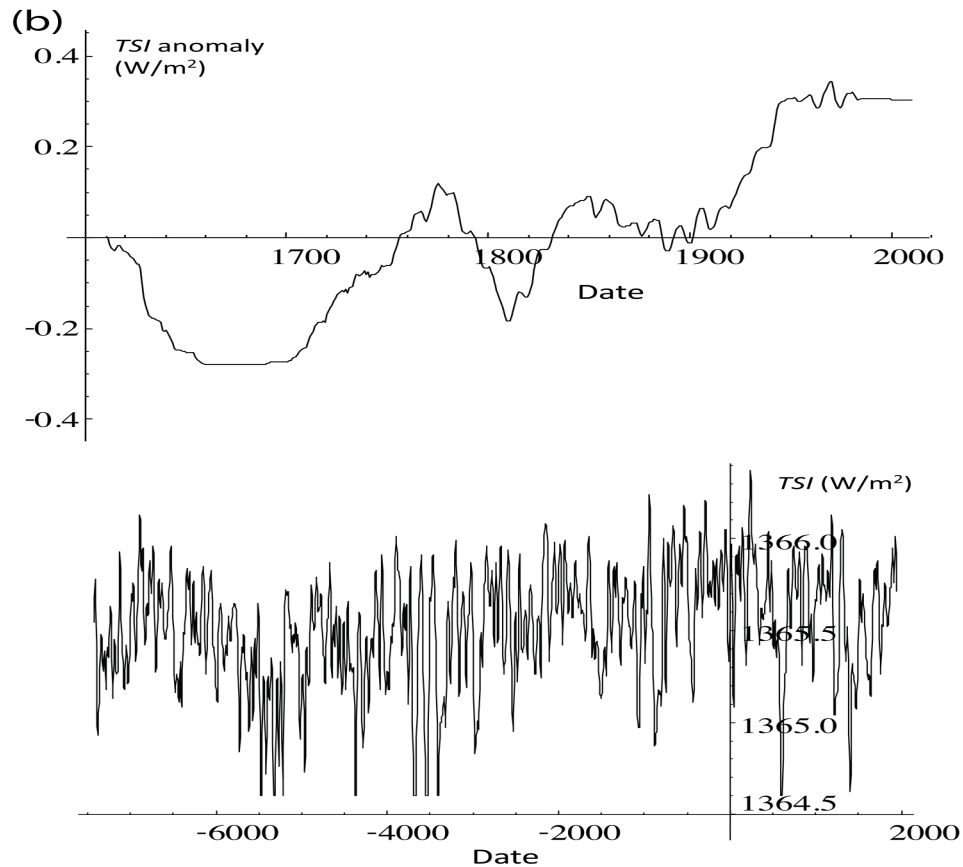


17

18 **Figure 2a.** The RMS Haar fluctuation $S(\Delta t)$ for the solar and volcanic reconstructions used in the ZC
 19 simulation for lags Δt from 2 to 1000 years (left). The solar is a “hybrid” obtained by “splicing” the
 20 sunspot-based reconstruction (Fig. 2b, top) with a ^{10}Be based reconstruction (Fig. 2b, bottom). The two
 21 rightmost curves are for two different ^{10}Be reconstructions (Shapiro et al., 2011; Steinhilber et al., 2009).
 22 Although at any given scale, their different assumptions lead to amplitudes differing by nearly a factor of
 23 10, their exponents are virtually identical and the amplitudes diminish rapidly with scale.

24

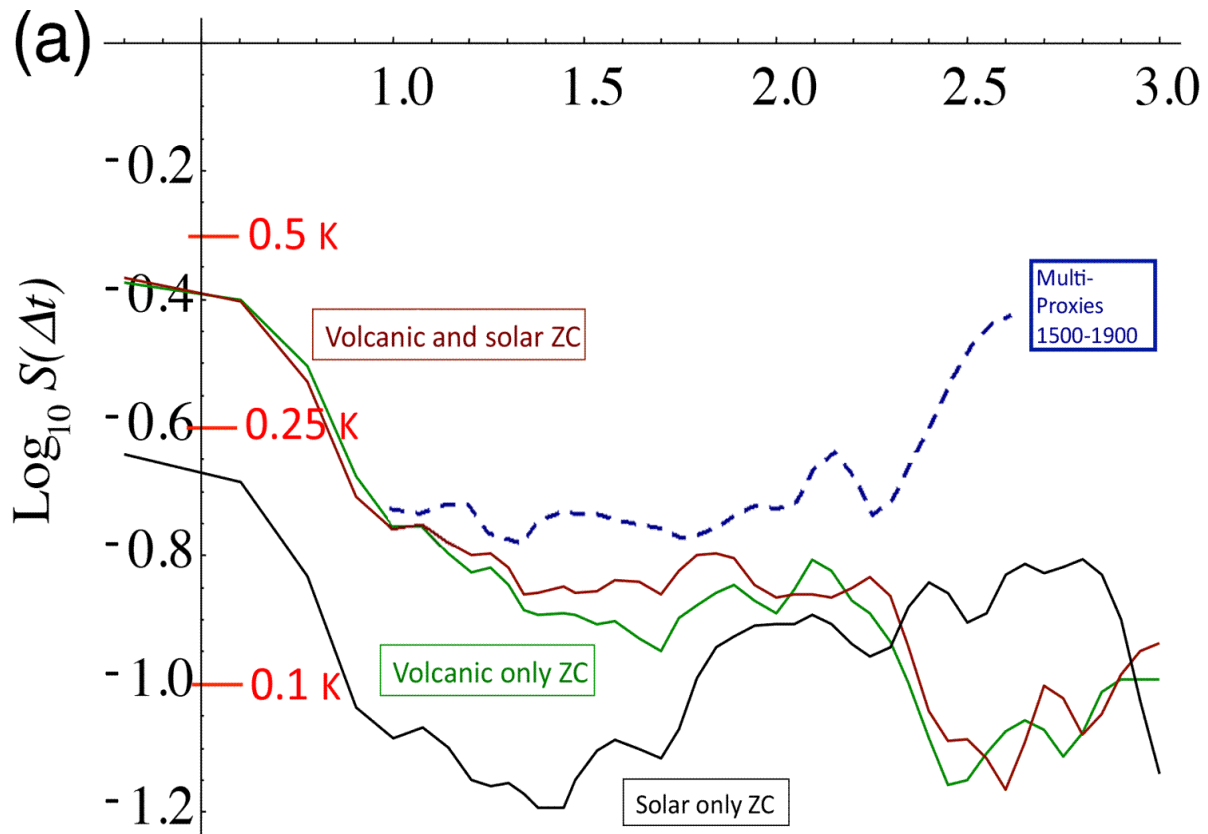
25



}26

}27 **Figure 2b.** A comparison of the sunspot derived Total Solar Irradiance (TSI) anomaly (top, used in the ZC
 }28 and GISS simulations back to 1610, $H \approx 0.4$) with a recent ^{10}Be reconstruction (bottom, total TSI - mean
 }29 plus anomaly - since 7362 BC, see Fig. 2a for a fluctuation analysis, $H \approx -0.3$) similar to that “spliced” onto
 }30 the sunspot reconstruction for the period 1000-1610. We can see that the statistical characteristics are
 }31 totally different with the sunspot variations “wandering” ($H > 0$) whereas the ^{10}Be reconstruction is
 }32 “cancelling” ($H < 0$). The sunspot data were for the “background” (i.e. with no 11 year cycle, see Wang et
 }33 al., 2005 for details), the data for the ^{10}Be curve were from Shapiro et al., (2011).

}34



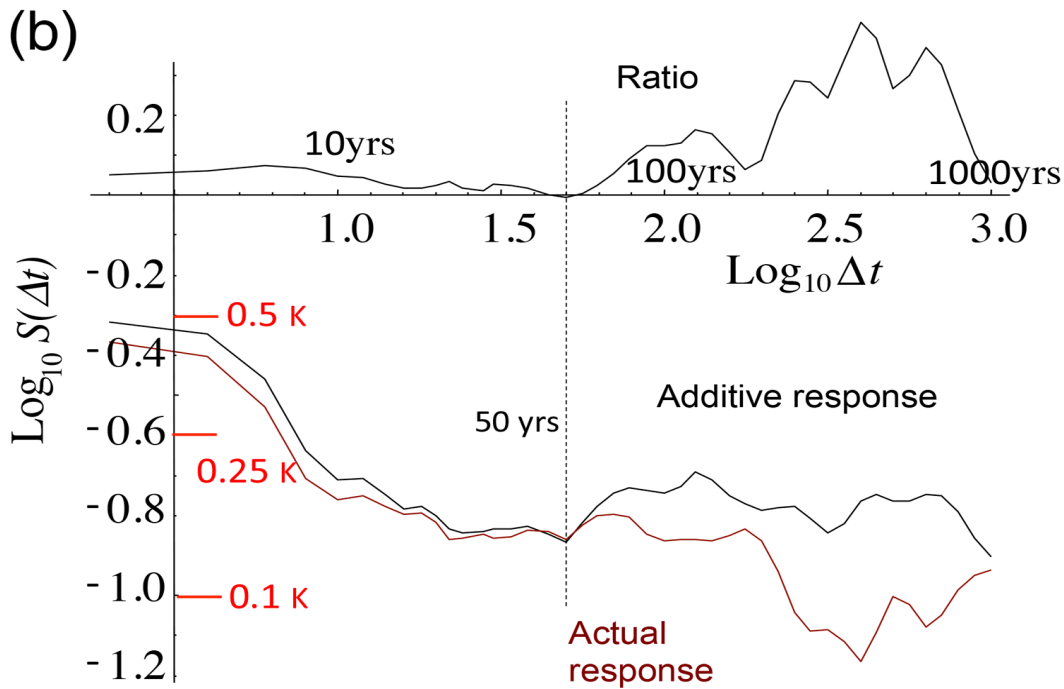
335

336

337

338 **Figure 3a.** The RMS Haar fluctuations of the Zebiak–Cane (ZC) model responses (from an ensemble of
 339 100 realizations) with volcanic only (green, from the updated Crowley reconstruction), solar only (black,
 340 using the sunspot based background (Wang et al., 2005), and both (brown). No anthropogenic effects were
 341 modelled. Also shown for reference are the fluctuations for three multiproxy series (blue, dashed, from
 342 1500-1900, pre-industrial, the fluctuations statistics from the three series were averaged, this curve was
 343 taken from Lovejoy and Schertzer, 2012b). We see that all the combined volcanic and solar response of the
 344 model reproduces the statistics until scales of ≈ 50 -100 years; however at longer time scales, the model
 345 fluctuations are substantially too weak – roughly 0.1K (corresponding to ± 0.05 K) and constant or falling,
 346 whereas at 400 yr scales, the temperature fluctuations are ≈ 0.25 K (± 0.125) and rising.

347



348

349

350

351 **Figure 3b.** A comparison of the RMS fluctuations of the ZC model response to combined solar and
 352 volcanic forcings (brown, bottom, from Fig. 3a), with the theoretical additive responses (black, bottom) as
 353 well as their ratio ($S_{\text{additive}} / S_{\text{actual}}$ black, top). The additive response was determined from the root mean
 354 square of the solar only and volcanic only response variances (from Fig. 3a): additivity implies that the
 355 fluctuation variances add (assuming that the solar and volcanic forcings are statistically independent). We
 356 can see that after about 50 years, there are strong negative feedbacks, the solar and volcanic forcings are
 357 subadditive, see Fig. 3c for a blow up of the ratio.

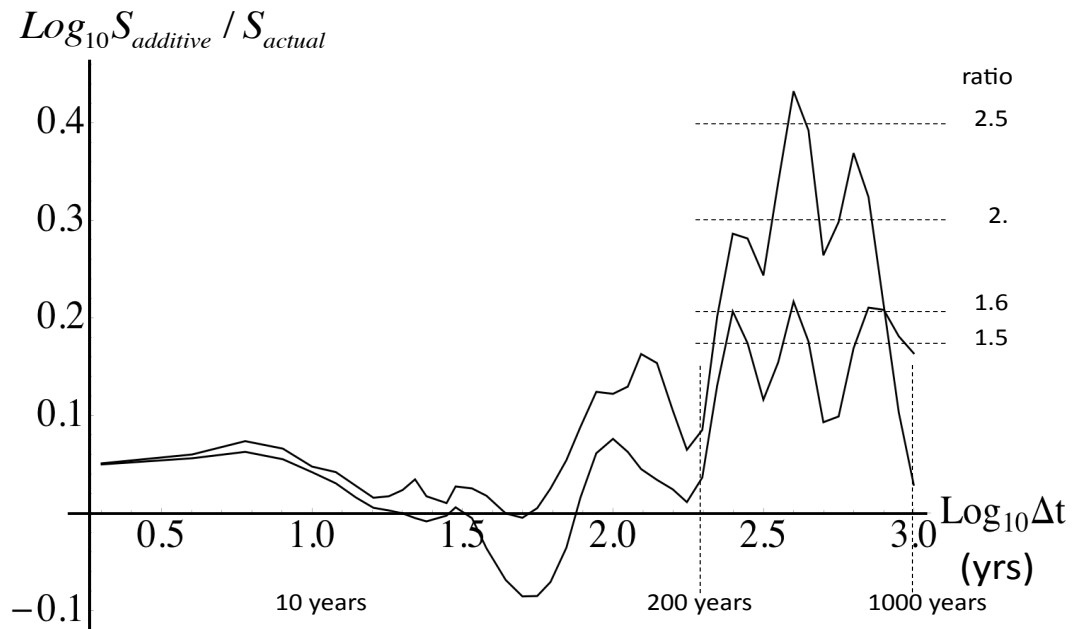
358

359

360

}61

(c)

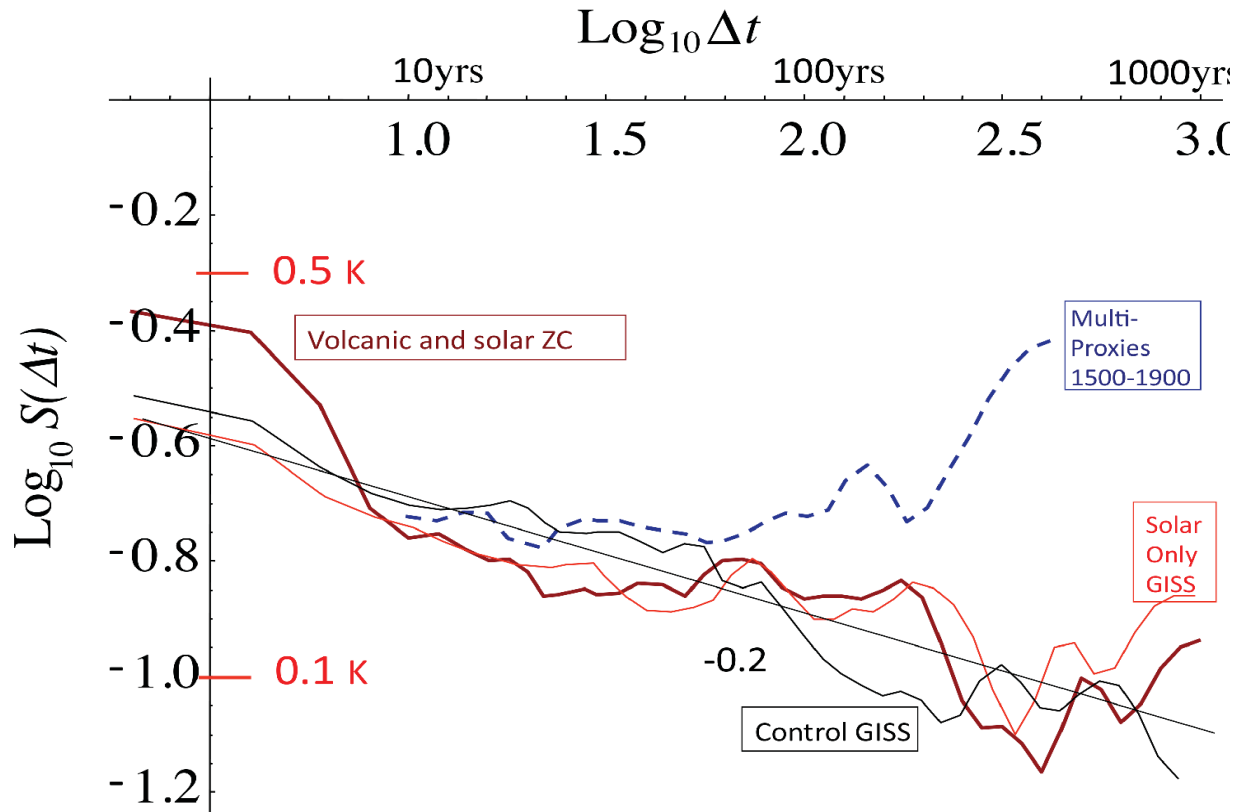


}62

}63 **Figure 3c.** An enlarged view of the ratio of the linear to nonlinear responses (from Fig. 3b). The top curve
 }64 assumes for the combined forcing, the linearity of the response and statistical independence of the solar and
 }65 volcanic forcings, whereas the bottom curve assumes only that the combined response to the forcing is
 }66 linear uses the actual response to the combined forcings. The maximum at around 400 yrs (top curve)
 }67 corresponds to a factor ≈ 2 (≈ 1.5 , bottom curve) of negative feedback between the solar and volcanic
 }68 forcings. The decline at longer durations (Δt 's the single 1000 yr fluctuation) is likely to be an artefact of
 }69 the limited statistics at these scales.

}70

}71

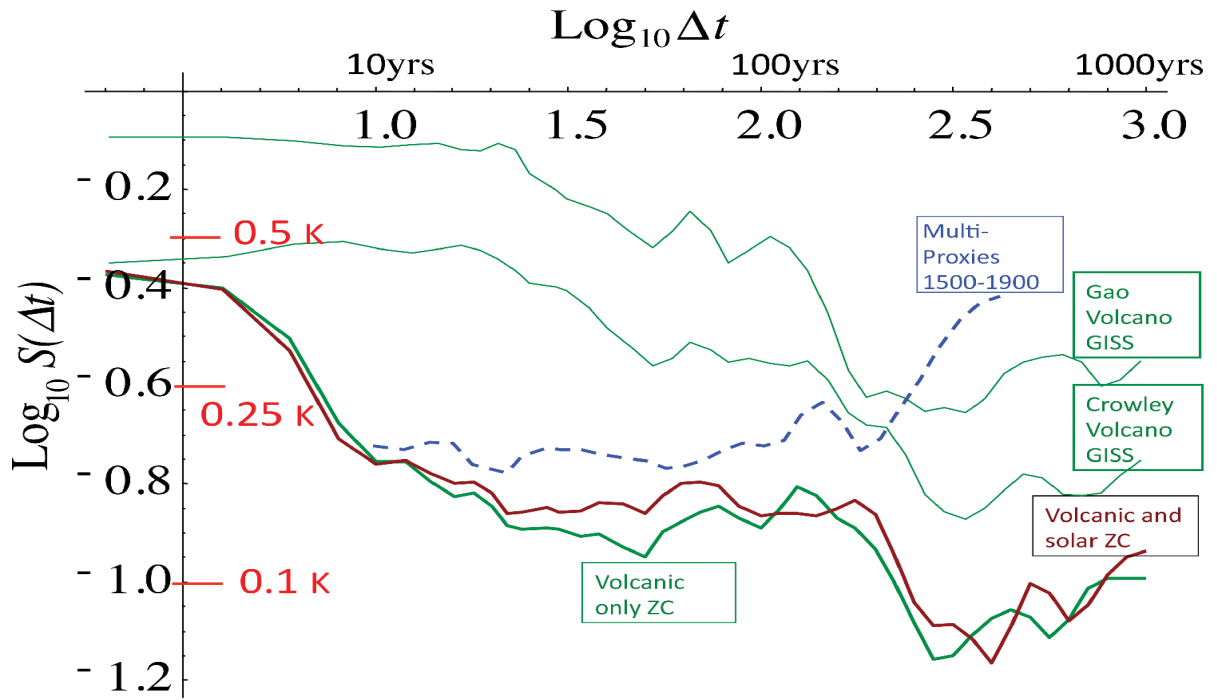


}72

}73

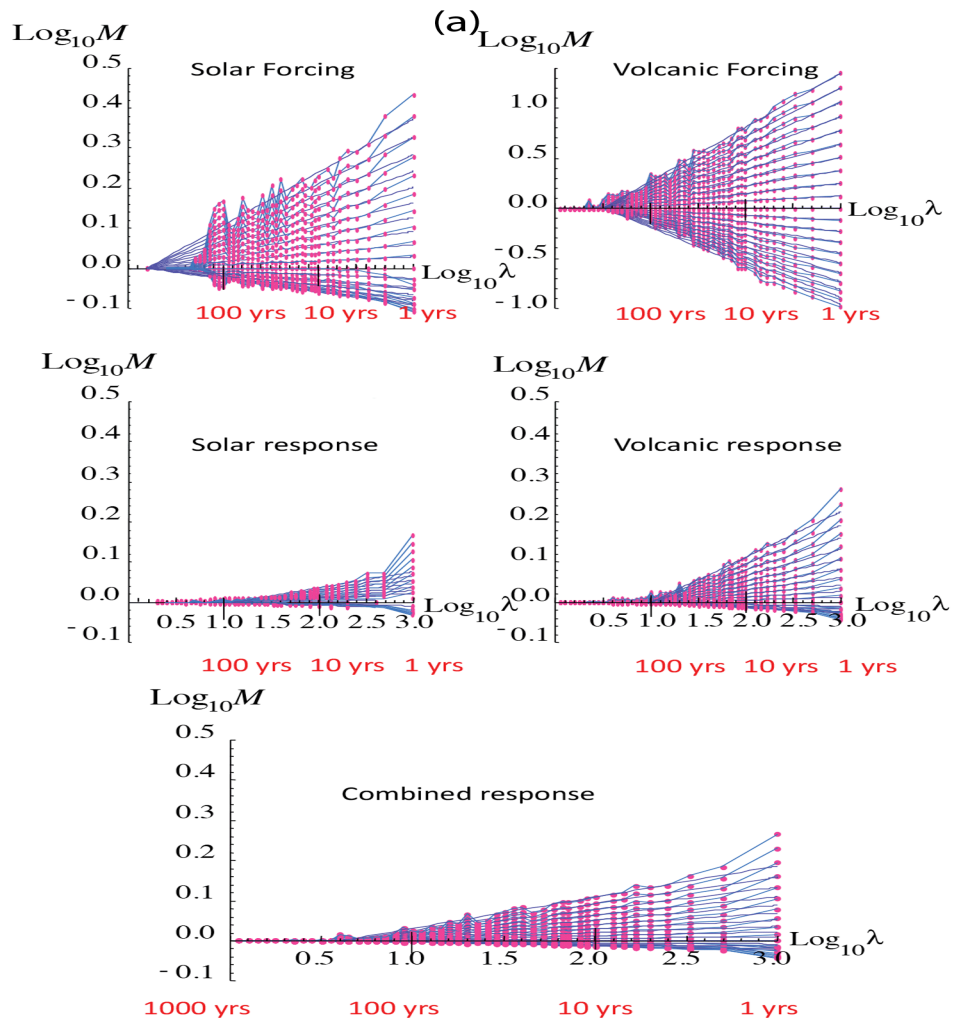
}74 **Figure 4.** A comparison of the Zebiak-Cane (ZC) model combined (volcanic and solar forcing) response
 }75 (thick brown) with GISS-E2-R simulations with solar only forcing (red) and a control run (no forcings,
 }76 black), the GISS structure functions are for land, northern hemisphere, reproduced from Lovejoy et al.,
 }77 (2013).

}78



382 **Figure 5.** A comparison of the volcanic forcings for the ZC model (bottom green) and for the GISS-E2-R
 383 GCM for two different volcanic reconstructions (Gao et al., 2008, and Crowley, 2000) (top green curves,
 384 reproduced from Lovejoy et al., 2013). Also shown is the combined response (ZC, brown) and the
 385 preindustrial multiproxies (dashed blue).

386



}87

}88

}89 **Figure 6a.** Analysis of the fluxes/cascade structures of the ZC forcings (top row) and ZC temperature
 }90 responses (middle, bottom rows); the normalized trace moments (Eq. (11)) are plotted for $q = 2, 1.9, 1.8,$
 }91 $1.7, 1.6, \dots 0.1$. Upper left is solar forcing (last 400 yrs only, mostly sunspot based), upper right is volcanic,
 }92 middle left, solar response (last 400 yrs), middle right (volcanic response), lower left, response to combined
 }93 forcings (last 1000 yrs). Note that all axes are the same except for volcanic. For the solar, only the last 400
 }94 yrs were used since this was reconstructed using the more reliable sunspot based method. The earlier ^{10}Be
 }95 based reconstruction had relatively poor resolution and is not shown. Since the volcanic variability was so
 }96 dominant, for the combined response (bottom left) the entire series was used. The red points and lines are
 }97 the empirical values, the blue lines are regressions constrained to go through a single outer scale point, see
 }98 eq. (11). In comparing the different parts of the figure, note in particular i) the log-log linearity for different
 }99 statistical moments, ii) the fact that the lines for different moments reasonably cross at a single outer scale,

and iii) the overall amplitude of the fluctuations – for example by visually comparing the range of the $q = 2$ moments (the top series) as we move from one graph to another.

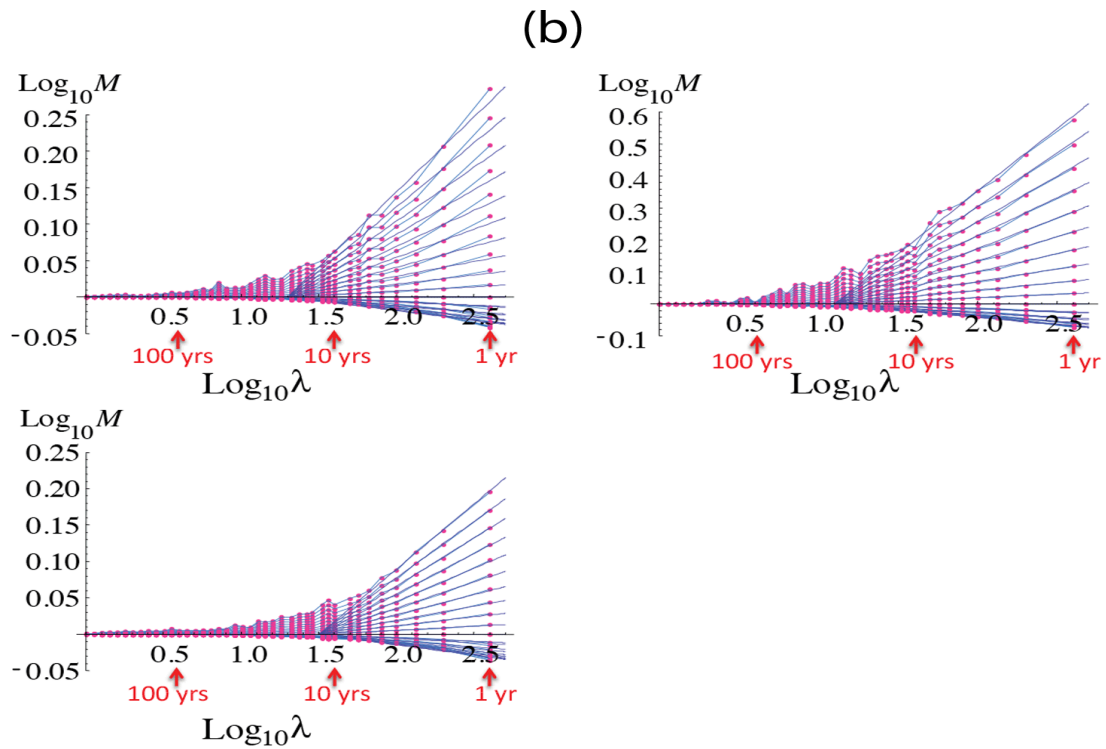
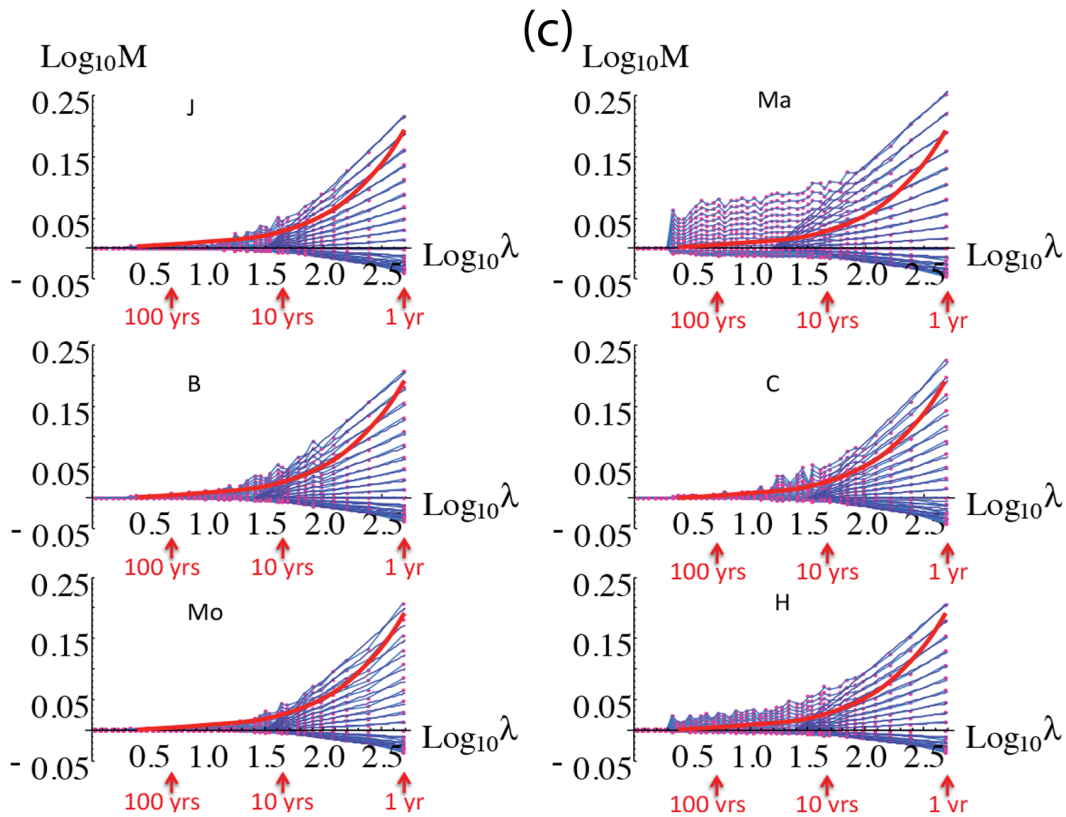


Figure 6b. The above shows the responses for the GISS-E2-R simulations (northern hemisphere, land, 1500-1900), $\lambda=1$ corresponds to 400 yrs. The upper left is for the response to the Crowley reconstructed volcanic forcings (same as used in the ZC simulations, not the change in the vertical scale), the upper right for the Gao reconstructed volcanic forcings and the lower left is for the solar only (mostly sunspot based, same as used in the ZC simulations).



021 **Figure 6c.** Trace moment analysis of six annual resolution multiproxies, J = Jones, Ma = Mann 98, B =
 022 Briffa, C = Crowley, Mo = Moberg, H = Huang, the curves are reproduced with permission from figure
 023 11.8, of Lovejoy and Schertzer, (2013), where full details and references are given. All were for the pre-
 024 industrial period 1500-1900 AD; $\lambda=1$ corresponds to 400 yrs. The curve shows the generic convergence of
 025 the envelope of curves to a quasi-Gaussian process, the proximity of the curve to the envelope indicates
 026 that with the possible exception of the Mann curve, the intermittency is low.